Title
Opioids depress breathing through action on two brainstem sites: circuit and molecular mechanisms

Author
Bachmutsky, Iris

Publication Date
2022

Peer reviewed|Thesis/dissertation

Opioids depress breathing through action on two brainstem sites: circuit and molecular mechanisms

by
Iris Bachmutsky

DISSERTATION
Submitted in partial satisfaction of the requirements for degree of
DOCTOR OF PHILOSOPHY

in

Neuroscience

in the

GRADUATE DIVISION
of the
UNIVERSITY OF CALIFORNIA, SAN FRANCISCO

Approved:

DocuSigned by:
David Julius
3CE818B8BD6645C...

David Julius
Chair

DocuSigned by:
Kevin Yackle
DocuSigned by:
Zachary Knight
DocuSigned by:
Massimo Scanziani
4AF406E430B7472...

Kevin Yackle

Zachary Knight

Massimo Scanziani

David Julius

Committee Members

Acknowledgements

When my parents left behind their families and moved across continents with two little kids, they knew that they were sacrificing in the hope that me and my brother would get to grow up safely on the other side of the American Dream. Even though some people say the American Dream is dead, and maybe it is inaccessible to most, my parents were able to find a place where a public education could carry me all the way from childhood to a PhD in one of the best Neuroscience programs in the world. Maybe they also hoped the American Dream would include making a little more money than they did, but hopefully they'll be happy with a PhD instead.

So, to my parents Alexander and Lilach Bachmutsky, thank you, I love you, I couldn't have done it without your sacrifice.

And to my brother Roi, who was always the goal I aspired to: without trying to catch up to you I certainly wouldn't have made it this far. Thank you, I love you.

I would also like to thank the wonderful scientific community at UCSF and the especially wonderful lab neighborhood I managed to park myself in these six years. I believe wholeheartedly that open office doors are an invitation to think together, and that being gracious with your reagents and time always pays back dividends. That's easy for me to say, however, when I don't have an office door to close and was more often receiving help than giving it. Lucky for me then that this philosophy was lived and breathed by every member of the adjoining labs of the Genentech Hall second floor, from the top down. In the best place to do science, this neighborhood is the best of the best.

I also want to thank my fellow graduate students in the Neuroscience program, which now include some of my dearest friends, for their generosity and kindness. Any time I reached out for help I found it. Any time I needed to rant, there was a willing ear.

For scientific advice I want to especially thank James Grove, Ray Dunn, Joshua Brenner and Eszter Kisch, who talked science with me in and out of work. You are the future of science I most look forward to.

And to my thesis committee members David Julius, Zachary Knight, and Massimo Scanziani, I am in your debt both for your scientific feedback and for always being available for advice when asked.

Most labs meet to talk about their projects once a week. For better or worse, the Yackle lab has always found itself gathered around in front of the window, drawing figures in whiteboard marker, on a near daily basis. I blame Kevin, mostly. Those conversations will always be my favorite part of being in the Yackle lab, so thank you all for always being willing to talk it out.

I would like to especially thank Adelae Durand, who was instrumental in the execution of my 2021 eLife paper and I am so grateful for all the time and effort she spent gathering data for that project. Matt Collie taught me how to cut slices and shared in my frustration when we naloxone-bombed each of the rigs, one at a time. And to Paul Wei who was my bench-neighbor for most of our PhDs: you were incredibly generous with your time and knowledge, and I thank you so much for your input over these six years. I also appreciate that in Matt's absence, when Kevin needed a new verbal punching bag, you bravely stepped up to the plate. I'm excited to see who's next in line.

When I joined the Yackle lab, I was the third student, and fifth member, of the burgeoning group. I was young and scared that even though I knew how to talk about science, I knew nothing about turning small experiments into important projects. Within my first year I took

up my thesis project, on opioid-induced respiratory depression, and that ended up being the scaffold around which I built my understanding of how to be a scientist. Kevin taught me to find the simplest, most straightforward experiments and to always plan ahead for the experiments a few months down the road. Eventually what felt like a handful of experiments coalesced into a paper and gave me faith that if I tackle a question one experiment at a time the disparate strands will weave into a coherent story.

When that paper was coming together, Kevin and I would drop by Roger Nicoll and David's offices for advice, and I felt like I was being given the opportunity to learn at the feet of giants. To David and Roger: I will always be grateful for your scientific advice and the ability you both had to make navigating the strange waters of the publishing process fun rather than stressful. I find myself quoting some of the advice you gave me in that period often, and I thank you wholeheartedly for the continued mentorship.

Oddly, I think the most important lesson I learned in my training was how to get excited about imperfect preliminary data. It seems simple, but while I was always in love with the craftsmanship of doing science, I was too much of a perfectionist with the product of my labor. Some scientists stress the importance of being critical of our data without acknowledging how very, very important it is to be excited about it first. If the moment you find something new doesn't fill you up with joy, there's no amount of success that can replace that moment retroactively. When I find myself unsure of whether the data is 'good enough' I send it to Kevin, who is invariably excited about it. From a place of excitement and motivation we can, and did, work out a plan to make it better.

Contributions

Chapter 1 is written by Iris Bachmutsky.

Chapter 2 is reproduced in an adapted form from:

> *Bachmutsky, I.*, Wei, X. P., Kish, E., & Yackle, K. (2020). Opioids depress breathing through two small brainstem sites. Elife, 9, e52694.*

I.B., E.K., & K.Y. Designed Research; I.B., & X.P.W. Performed Research; I.B., X.P.W. Analyzed Data; I.B., & K.Y. Wrote Paper.

Chapter 3 is reproduced in an adapted form from:

> Bachmutsky, I.*, Wei, X. P., Durand, A., & Yackle, K. (2021). ß-arrestin 2 germline knockout does not attenuate opioid respiratory depression. *Elife*, *10*, e62552.

I.B. & K.Y. Designed Research; I.B., X.P.W., & A.D. Performed Research; I.B. Analyzed Data; I.B. & X.P.W. Wrote Paper.

Chapter 4 is written by Iris Bachmutsky.

“So it goes.”

-Kurt Vonnegut

Opioids depress breathing through action on two brainstem sites: circuit and molecular mechanisms

Iris Bachmutsky

Abstract

Opioids are perhaps the most effective analgesics in medicine. However, between 1999 and 2020, over 500,000 people in the United States died from opioid overdose. This health epidemic demands innovative solutions that will require uncovering the key brain areas and cell types mediating the cause of overdose— opioid-induced respiratory depression. Here, I identify two primary changes to breathing after administering opioids. These changes implicate the brainstem's breathing circuitry which I confirm by locally eliminating the μ-Opioid receptor. I find the critical brain site is the preBötzinger Complex, where the breathing rhythm originates, and use genetic tools to reveal that just 70–140 neurons in this region are responsible for its sensitivity to opioids. Meanwhile, in the absence of this basic understanding of the mechanisms mediated opioid respiratory depression, some groups have already moved forward with development of therapeutics with novel biochemical properties they claim will dissociate opioid-like analgesia from effects on breathing. One such approach has been the design of so-called 'biased agonists' that signal through some, but not all pathways downstream of the μ-opioid receptor (MOR), the target of morphine and other opioid analgesics. This rationale stems from a study suggesting that MOR-induced ß-arrestin 2 dependent signaling is responsible for opioid respiratory depression, whereas adenylyl cyclase inhibition produces analgesia. To verify this important result that motivated the 'biased agonist' approach, I re-examine breathing in ß-arrestin 2-deficient mice and instead find no connection between ß-arrestin 2 and opioid respiratory depression. Put together, this work suggests a new approach to develop safer opioid-like drugs is needed, and that future characterization of the small group of neurons

mediating respiratory depression may lead to novel therapies that prevent respiratory side effects while sparing analgesia.

Table of Contents

List of Figures

Chapter 2:

List of Tables

Chapter 1:

Introduction

The opioid epidemic in the United States has caused more than 500,000 deaths since 1999, with the number of deaths steadily increasing each year with few exceptions (1). Various stages of the epidemic have been driven by the development and distribution of increasingly potent opioid drugs. Most recently, the introduction of the synthetic opioid drug fentanyl, and its analogs, have caused a sharp acceleration in drug overdose deaths and led to the official designation of the opioid epidemic in 2017 as a public health emergency (2).

Despite substantial efforts to resolve this crisis opioid treatment remains rare and expensive, and the primary therapeutic, naloxone, can only be used acutely at the time of crisis. Basic science, medicine, and public policy each bear a heavy responsibility to introduce new avenues to address this epidemic. From a basic science perspective, a better understanding of how opioids exert their lethal effects may enable us to develop safer opioid drugs and prevent overdose.

Death from opioid overdose results from slow and shallow breathing, also known as opioid-induced respiratory depression (OIRD, *3*). These opioid drugs act on receptors expressed both centrally and peripherally to exert their effects, including directly on ponto-medullary brain centers that control breathing (4,5). The relative contribution of each of these small brainstem nuclei is unknown and may guide future drug discovery. Additionally, the novel development of ‘biased agonist’ opioid drugs has promised to dissociate negative lethal effects of opioids, due to respiratory depression, from their positive analgesic effects (6). However, this bold idea was founded on a claim that OIRD was mediated by the downstream ß-arrestin 2 signaling pathway that has somehow evaded critical evaluation (7). Given the importance of this claim, the role of ß-arrestin 2 signaling in OIRD must be re-examined.

More broadly, the impact of opioid drugs on the breathing central pattern generator may shine a new light on how this unique pattern generator orchestrates its rhythm. Historically, the field of central pattern generator (CPG) rhythmogenesis has settled on some common principles of organization. These include common intrinsic cellular properties and connectivity schemes. The simplest mechanism with which to generate a rhythm is to employ a pacemaker neuron, or group of neurons, to set the pace. This is similar to how the sinoatrial node paces heart rate. These signals can then be propagated to other neurons through electrical coupling, like in the heart, or chemical synapses. In the extensively studied pyloric rhythm generator of the crustacean stomatogastric (STG) ganglion, pace-making neurons connected through reciprocal inhibition generate synchronous activity in what is called the 'half-center' model of rhythmogenesis (8). Other well-established CPGs controlling diverse processes, such as locomotion and swimming, rely on combinations of pacemaker neurons, reciprocal inhibition, and electrical coupling with various iterations.

The mammalian breathing rhythm generator is somewhat unique in the conception of its rhythmogenic mechanism. The current dogma contends that the rhythm is generated by the recurrent excitatory drive of a sparse network of excitatory neurons located within the breathing CPG, a brainstem nucleus called the preBötzinger Complex (preBötC) (11,12). When this nucleus is disconnected from downstream areas in intact mice the breathing rhythm is abolished, and slices containing the preBötC autonomously generate respiratory-like rhythmic activity. To date, no pacemaker neurons have been recognized for this system and rhythm generation persists in the absence of any inhibition (9,10). While some molecular markers have been found to label neurons modulating the breathing rhythm, no key cell type has been identified to play a specialized rhythmogenic role (13). And yet, while only a small proportion of neurons in the region are opioid sensitive, the rhythmic firing of the preBötC *in vitro* is abolished by administration of opioid agonists (14). If these neurons enable the sensitization of breathing to opioids in cases of lethal overdose, this suggests that even *in vivo* inhibition of such a small

number of neurons is sufficient to block respiratory rhythmogeneisis. Could this small number of neurons represent an as-of-yet unidentified molecular marker for the rhythogenic kernel of the preBötC? Alternatively, the current model would suggest that, since no neuron plays a particularly specialized role in rhythmogenesis, removing any similarly sized group of glutamatergic neurons from the network would destabilize the respiratory rhythm. This would be a puzzling architecture for a network that generates a rhythm as vital as breathing. However, some current in vitro studies provide support for this idea (15). Whether these mu-opioid receptor expressing neurons upend the current model of breathing rhythm generation or not, they certainly present an intriguing candidate for further study.

References

1. National Institute on Drug Abuse. (2022, January 20). Overdose Death Rates. Retrieved November 15, 2022, from https://nida.nih.gov/research-topics/trends-statistics/overdose-death-rates
2. Allen and A. Kelly. (2017, Oct. 26). Trump Administration Declares Opioid Crisis A Public Health Emergency. NPR. Retrieved November 15, 2022, from https://www.npr.org/2017/10/26/560083795/president-trump-may-declare-opioid-epidemic-national-emergency
3. K.T. Pattinson, Opioids and the control of respiration. *Br J Anaesth. 6,* 747-758 (2008).
4. A. Mansour, C.A. Fox, S. Burke, F. Meng, R.C. Thompson, H. Akil, S.J Watson, Mu, delta, and kappa opioid receptor mRNA expression in the rat CNS: an in situ hybridization study. *Journal of Comparative Neurology*, *350*, 412-438 (1994)
5. G.C. Kirby, D.S. McQueen, Characterization of opioid receptors in the cat carotid body involved in chemosensory depression in vivo. *British journal of pharmacology*, *88*, 889-898 (1986).
6. Hill R, Disney A, Conibear A, Sutcliffe K, Dewey W, Husbands S, Bailey C, Kelly E, Henderson G. 2018. The novel μ-opioid receptor agonist PZM21 depresses respiration and induces tolerance to antinociception. *British journal of pharmacology* 175:2653–2661. doi:10.1111/bph.14224.
7. Hill R, Disney A, Conibear A, Sutcliffe K, Dewey W, Husbands S, Bailey C, Kelly E, Henderson G. 2018. The novel μ-opioid receptor agonist PZM21 depresses respiration and induces tolerance to antinociception. *British journal of pharmacology* 175:2653–2661. doi:10.1111/bph.14224.
8. Marder, E., & Calabrese, R. L. (1996). Principles of rhythmic motor pattern generation. *Physiological reviews*, *76*(3), 687-717.

9. Murakoshi T, Otsuka M. 1985. Respiratory reflexes in an isolated brainstem-lung preparation of the newborn rat: possible involvement of gamma-aminobutyric acid and glycine. Neurosci. Lett. 62:63– 68
10. McCrimmon D, Mellen N, Feldman J. 1996. Lung inflation-induced expiratory lengthening requires GABAA receptor activation in a lung attached in vitro brainstem-spinal cord preparation. Soc. Neurosci. Abstr. 22:1596
11. J.C. Smith, H.H. Ellenberger, K. Ballanyi, D.W. Richter, J.L. Feldman, Pre-Bötzinger complex: a brainstem region that may generate respiratory rhythm in mammals. *Science*, *254*, 726-729 (1991).
12. J.L. Feldman, C.A. Del Negro, P.A. Gray, Understanding to rhythm of breathing: so near, yet so far. *Annu Rev Physiol., 75*, 423-452 (2013).
13. Yackle, K. (2022). Transformation of Our Understanding of Breathing Control by Molecular Tools. *Annual Review of Physiology*, *85*.
14. G. Montandon, W. Qin, H. Liu, J. Ren, J.J. Greer, R.L. Horner, PreBotzinger complex neurokinin-1 receptor-expressing neurons mediate opioid-induced respiratory depression. *J Neurosci., 31*, 1292-1301 (2011).
15. Wang, X., Hayes, J. A., Revill, A. L., Song, H., Kottick, A., Vann, N. C., ... & Del Negro, C. A. (2014). Laser ablation of Dbx1 neurons in the pre-Bötzinger complex stops inspiratory rhythm and impairs output in neonatal mice. *Elife*, *3*, e03427.

Chapter 2:

Opioids depress breathing through two small brainstem sites

Introduction

Nearly 400,000 people in the United States died from a drug overdose involving a prescription or illicit opioid between 1999 and 2017 (*1*). This epidemic is not unique to the United States and with the increasing distribution of highly potent synthetic opioids like fentanyl, it has become a global public health emergency (*2*). Death from opioid overdose results from slow and shallow breathing, also known as opioid induced respiratory depression (OIRD, *3*). Like humans, breathing in mice is severely depressed by opioids and this response is eliminated when the μ-Opioid receptor (*Oprm1*) is globally deleted (4). *Oprm1* is broadly expressed, in both the central and peripheral nervous systems, including sites that could modulate breathing such as: the cerebral cortex, brainstem respiratory control centers, primary motor neurons, solitary nucleus, and oxygen sensing afferents (*5,6*). Therefore, either one or multiple sites could be mediating the depressive effects of opioids on breathing.

Indeed, multiple brain regions have been shown to independently slow breathing after local injection of opioid agonists (*6-9*). Although informative, doubts remain for which of these sites are necessary and sufficient to induce OIRD from systemic opioids for three reasons. First, injection of opioid agonists or antagonists into candidate areas modulates μ-opioid receptors on the cell body (post-synaptic) as well as receptors on incoming terminals (pre-synaptic). Second, these studies necessitate anesthetized and reduced animal preparations which alters brain activity in many of the candidate *Oprm1* expressing sites. And third, there is not a standard and quantitative definition for how breathing changes in OIRD and this makes comparing studies that use different breathing metrics measured in different experimental paradigms challenging.

To address these limitations, we conducted a detailed quantitative analysis of OIRD in awake animals and identify two key changes to the breath that drive the depressive effects of opioids. These two metrics thereafter define OIRD in our study and can serve as a rubric for others. We then locally eliminate the μ-opioid receptor in awake mice, disambiguating pre and post-synaptic effects, and use these metrics to define two key brain sites that mediate OIRD. Recently, a similar approach demonstrated some role for these sites in OIRD (*10*). Among these two sites in our study, we find that one is dominant and driven by just 140 critical neurons *in vitro* and, importantly, these neurons are not required for opioid-induced analgesia, suggesting a neutral target for developing safer opioids or rescue strategies for opioid overdose.

Results

Up to now, OIRD has generally been described as a slowing and shallowing of breath (*3*). We therefore felt it was important to more precisely, quantitatively describe the changes in breathing in hopes of elucidating potential mechanisms of respiratory depression. We began by asking whether specific parameters of the breath are affected by opioids. We monitored breathing in awake, behaving mice by whole body plethysmography after intraperitoneal injection (IP) of saline for control and then 20 mg/kg morphine at least 24 hours later (Fig. 2.1A). Compared to saline, breathing after morphine administration (in normoxia) became much slower and inspiratory airflow decreased, each by 60% (Fig. 2.1B,C). This culminated in ~50% decrease in overall minute ventilation (MV = approximated tidal volume x respiratory rate, Fig. 2.1C), demonstrating that 20 mg/kg morphine is, indeed, a suitable dose to model OIRD.

Breath morphology in normoxia after IP saline versus morphine cannot be directly compared since activity of the mouse is different (exploring vs. sedated, Movie S1-2), which significantly influences the types of breaths taken. This prevented a precise characterization of breath parameters that dictate OIRD. To overcome this, we measured breathing in hypercapnic air (21% O_2, 5% CO_2) which normalizes behavior and thus breathing (Fig. 2.1D, Movie S3-4).

As in normoxia, morphine depressed respiratory rate (by 50%, Fig. 2.1E,F), peak inspiratory airflow (by 60%, Fig. 2.1E,F), and minute ventilation (by 60%, Fig. 2.1F). Hypercapnic breaths after saline exhibited two phases, inspiration and expiration, each lasting about 50 msec. (Fig. 2.1G,H). After morphine, only the inspiratory phase (measured as inspiratory time, Ti) became substantially longer (Fig. 2.1G,H). Additionally, hypercapnic breaths showed a new, third phase after the initial expiration (measured as expiratory time, Te, Fig. 2.1G,H) that was characterized by prolonged little to no airflow (<0.5mL/sec.) preceding hypercapnia induced active expiration (*11*). We define this new phase as a pause (low airflow + active expiration, Fig. 2.1G, Fig. 2.5). Such pauses lasted up to several hundred milliseconds (Fig. 2.1I) and accounted for about one-third of the average breath length (Fig. 2.1J). Thus, the 50% decrease in respiratory rate after morphine administration is primarily due to prolonging of Ti and pause phases, and the increased prevalence of time spent in pause significantly contributes to the decrease in minute ventilation.

Typically, the length of inspiratory time is determined by a stretch-evoked feedback signal from the lung which terminates inspiration (*12*). This reflex is represented by the correlation observed between Ti and peak inspiratory airflow (Fig. 2.1K). Breaths in morphine still maintain this correlation despite having a longer Ti and decreased inspiratory airflow (Fig. 2.1K). As a result, morphine breaths have a similar approximated tidal volume (TV) compared to saline control (Fig. 2.1L,M). In other words, as opioids decrease inspiratory airflow, Ti displays a compensatory increase to preserve TV (Fig. 2.1N, *13*). In summary, opioids cause only two primary changes to the breath, namely, 1) decreased inspiratory airflow and 2) addition of a pause phase that delays initiation of subsequent breaths (Fig. 2.1N). These two parameters can both be controlled by the breathing central pattern generator, the preBötzinger Complex (preBötC), in the brainstem and suggest that this may be a key locus affected during OIRD (*14-16*).

Indeed, the preBötC has been proposed to play a key role in OIRD since localized injection of opioids results in respiratory depression and localized naloxone reverses decreased breathing after administration of systemic opioids (*7,17*). However, such experiments fail to distinguish between the action of opioids on presynaptic terminals (*18*) of distant neurons projecting into the preBötC versus direct action on preBötC neurons themselves (Fig. 2.2A *7*,*19*,*20*). To overcome this, we genetically eliminated the μ-Opioid receptor (*Oprm1*) from preBötC cells exclusively, sparing projecting inputs, by stereotaxic injection of adeno-associated virus constitutively expressing Cre (AAV-Cre) into the preBötC of *Oprm1* flox/flox (*Oprm1*$^{f/f}$) adult mice (Fig. 2.2B). To establish a baseline, we first measured breathing after administration of saline and morphine in normoxia and hypercapnia in intact animals, as described above. At least one month after bilateral injection of virus into the preBötC, we then re-analyzed breathing (Fig. 2.2C). With this protocol, each animal's unique breathing and OIRD response serves as its own internal control, which is necessary due to the variability in OIRD severity between mice (Fig. 2.1F). Deletion of *Oprm1* in the preBötC did not affect breathing observed after saline injection (Fig. 2.2D,E), suggesting that in this context, opioids do not exert an endogenous effect. In contrast, breathing was markedly less depressed by morphine administration (Fig. 2.2D,E) compared to the intact control state: breaths were twice as fast (3 to 6 Hz, Fig. 2.2F,H), the peak inspiratory flow was larger (Fig. 2.2F,I), and pauses were nearly eliminated (Fig. 2.2G,J). Notably, histological analysis confirmed that AAV-Cre-GFP expression was localized to the preBötC (Fig. 2.7), and AAV-GFP or tdTomato injected control mice without removal of *Oprm1* showed no change in OIRD compared to the pre-injected control state (Fig. 2.2H-J), demonstrating that animals do not develop tolerance to opioids within our experimental timeline. Importantly, rescue of OIRD similarly occurred in normoxia (Fig. 2.8) and was also specific to breathing since opioids induced analgesia in tail-flick assay after deletion of *Oprm1* in the preBötC (Fig. 2.9).

Although key features of OIRD (inspiratory airflow and pause) were attenuated by preBötC AAV-Cre injection, rescue was incomplete. This could be explained by incomplete *Oprm1* deletion within the preBötC, or participation of another brain site in OIRD. Injection of opioids into the parabrachial (PBN)/Kolliker-Fuse (KF) nucleus can also slow breathing, making it a candidate second site (*8,9*). In fact, the PBN/KF has been proposed to be the key site mediating OIRD (*21,22*). We therefore took a similar approach to test the role of the PBN/KF in OIRD (Fig. 2.3A). AAV-Cre injection into the PBN/KF (Fig. 2.10) produced a slight increase in the morphine-evoked respiratory rate (Fig. 2.11, Fig. 2.3D,E) and inspiratory airflow (Fig. 2.11, Fig. 2.3F,G), but had a more moderate effect than injection into the preBötC.

To determine if the preBötC and PBN/KF can completely account for OIRD (Fig. 2.3A), we genetically deleted *Oprm1* from the preBötC and then from the PBN/KF (Cohort 1) or vice versa (Cohort 2, Fig. 2.3B). In either cohort, double deletion breathing after morphine administration looked nearly identical to that of saline control animals (Fig. 2.3C), with breathing rate and inspiratory airflow depressed by only ~20% compared to saline (Fig. 2.3D-G). Moreover, changes in breathing after viral injection at the second site appeared additive (Fig. 2.3D-G) and equivalent to individual preBötC (Fig. 2.2) or PBN/KF (Fig. 2.11, Fig. 2.3D-G) effects for each cognate cohort. The double deletion OIRD rescue was similar in normoxia (Fig. 2.12). To our surprise, rescues also occurred in animals which happened to have mostly unilateral PBN/KF AAV-cre transduction (Fig. 2.13), therefore these animals were still included in our double deletion analysis (Fig. 2.3E,G). Breathing in double-deleted animals was even resilient to super-saturating doses of opioid that severely slow breathing in control animals (150mg/kg fentanyl, Fig. 2.3H,I). Taken together, our data are consistent with a model in which both the preBötC and PBN/KF contribute to opioid respiratory depression, with the former being predominant, and together account for OIRD.

Given the relative importance of the preBötC to OIRD, we sought to identify which *Oprm1* expressing cells within this region depress breathing. Single cell transcriptome profiling

of the ventral lateral brainstem of P0 mice (Fig. 2.4A) showed that *Oprm1* (mRNA) is expressed almost exclusively by neurons (Fig. 2.14) and is remarkably restricted to just 8% of presumed preBötC neurons (Fig. 2.4B). This alone is interesting, as it suggests that modulation of only a small subset of neurons with the preBötC is enough to significantly impact its ability to generate a rhythm. We also determined that within the preBötC, *Oprm1* (mRNA) was expressed by glycinergic (*Slc6a5* expressing), gabaergic (*Gad2*/*Slc32a1* expressing), and glutamatergic (*Slc17a6* expressing) neural types alike (Fig. 2.4C) and therefore *Oprm1* (mRNA) expression is not exclusive to any known rhythmogenic preBötC subpopulation.

Slices containing the preBötC autonomously generate respiratory-like rhythmic activity *in vitro* which is depressed in both rate and amplitude by bath administration of opioid agonists (*20,23*), similar to opioid effects we observed on breathing *in vivo*. To determine which neural class mediates the depression of preBötC activity, we measured rhythmic bursting activity *in vitro* (Fig. 2.4D) after selectively genetically deleting *Oprm1* from each neural class. We achieved this deletion by crossing *Oprm1*$^{f/f}$ mice with each of the following: *Slc17a6*-Cre, *Slc32a1*-Cre, *Gad2*-Cre, or *Slc6a5*-Cre transgenic animals. preBötC slices from control mice (*Oprm1*$^{f/f}$, *Oprm1*$^{f/+}$, or *Oprm1*$^{+/+}$) burst every 5-10 seconds and this activity was eliminated in 100% of slices by bath application of the selective μ-Opioid receptor agonist [D-Ala^2, NMe-Phe^4, Gly-ol^5]-enkephalin (DAMGO, 50nM), and subsequently rescued by opioid antagonist naloxone (Fig. 2.4E,F). Strikingly, the bursting rhythm of *Slc17a6*-Cre;*Oprm1*$^{f/f}$ slices was not slowed by DAMGO, whereas the rhythm in *Gad2*-, *Slc32a1*-, and *Slc6a5*-Cre; *Oprm1*$^{f/f}$ slices was entirely eliminated, akin to wild type controls (Fig. 2.4E,F, Fig. 2.15). This demonstrates that glutamatergic excitatory neurons, representing ~50% of all preBötC *Oprm1*-expressing neurons and therefore 4% of preBötC neurons, mediate OIRD *in vitro*.

Next, we dissected the glutamatergic *Oprm1* preBötC neurons by two developmental transcription factors, *Dbx1* or *Foxp2* (*24-26*), to determine if a subset can rescue rhythm depression (Fig. 2.4G). Triple-labeling of *Dbx1*-YFP, OPRM1 fused to mCherry (OPRM1-

mCherry), and FOXP2 protein quantified within a single preBötC revealed three molecular subtypes of P0 *Oprm1* glutamatergic neurons: 92 ± 9 Dbx1, 50 ± 2 Dbx1/FOXP2, and 20 ± 4 FOXP2 (Fig. 2.4H,I). We selectively eliminated the μ-Opioid receptor in these two lineages (*Dbx1*-Cre;*Oprm1*$^{f/f}$ or *Foxp2*-Cre;*Oprm1*$^{f/f}$) and measured preBötC slice activity at increasing concentrations of DAMGO, exceeding the dose necessary to silence the control rhythm (500nM vs. 50nM). Elimination of *Oprm1* from both genotypes was sufficient to rescue the frequency and amplitude of preBötC bursting in DAMGO, and the Dbx1 rescue was comparable to elimination of *Oprm1* from all glutamatergic neurons, while the Foxp2 rescue was substantial, but partial (~50-60%, Fig. 2.4J). This shows that opioids silence a small cohort (~140) of glutamatergic neurons to depress preBötC activity, and that a molecularly defined subpopulation, about half, can be targeted to rescue these effects.

Discussion

Here we show that two small brainstem sites are sufficient to rescue opioid induced respiratory depression *in vivo*. Between them, the preBötC is the critical site and we molecularly define ~140 *Oprm1* glutamatergic neurons within that are responsible for this effect *in vitro*. Future study of these neurons will provide the first example of endogenous opioid modulation of breathing. Furthermore, characterization of these neurons and their molecular response to opioids may extend existing strategies (*27*) or reveal a novel strategy for separating respiratory depression from analgesia and therefore enable the development of novel opioids or related compounds that relieve pain without risk of overdose.

A rubric for studying opioid and other respiratory depressants

We find that although multiple breathing parameters are impacted by opioids, decreased inspiratory airflow and delayed breath initiation, which we term pause, represent the primary changes that result in OIRD. Pauses occur during expiration and account for tens to hundreds

of milliseconds of low airflow per breath. In hypercapnia, these pause periods terminate with an active expiration. The force, timing of inspiration, and expression of active expiration are ultimately determined by the inspiratory rhythm generator, the preBötC, and focused our initial studies to this site (*14-16,28*). Additionally, correlates of these two changes manifest as decreased burst size and frequency in the activity of the preBötC slice *in vitro.* These two key changes in the breath can guide future OIRD studies and efforts to characterize and test novel opioid drugs. Additionally, this workflow can be applied to the analysis of other respiratory depressants.

Just two small brainstem sites mediate OIRD

Our experimental design allowed us to determine that both the preBötC and PBN/KF have independent and additive rescue of OIRD. Of these two, the preBötC has the larger magnitude rescue of our two core breathing parameters. The combined deletion of μ-Opioid receptor from both sites essentially eliminates OIRD, even to extremely high doses of the potent opioid fentanyl. This suggests that targeting just these two sites is sufficient to rescue opioid respiratory depression. We interpret the small remaining effect of opioids we observe to be due to incomplete transduction of these brain areas but cannot rule out other minor contributing sites or morphine activation of δ and κ opioid receptors. Our studies were limited to two opioids (morphine and fentanyl) at a specific dose and it will be important in future work to determine if these two brain sites are also critical for OIRD caused by these opioids at different doses or other opioids altogether.

Depression of preBötC rhythm by silencing a small glutamatergic subpopulation

The two hallmark changes during OIRD, decreased inspiratory airflow and delayed initiation, perfectly match the opioid induced depression of amplitude and frequency in the preBötC slice. We show that ~140 *Oprm1* glutamatergic preBötC neurons mediate this effect. And surprisingly, half this number, just ~70 glutamatergic neurons are sufficient to rescue opioid depression of the preBötC rhythm (50 Dbx1/FOXP2 and 20 FOXP2 in *Foxp2*-Cre;*Oprm1*$^{f/f}$, Fig. 2.16). Further,

given the importance of Dbx1 neurons in respiratory rhythm generation (*24,25*), rescuing *Oprm1* in just ~50/140 Dbx1 neurons (the Foxp2+ subset) may be sufficient to prevent preBötC depression, the smallest number of neurons we propose. This small number is remarkably consistent with the number of Dbx1 neurons that must be lesioned to arrest preBötC activity (*29*). Given the similarity of these effects, we hypothesize that opioids are primarily acting by silencing presynaptic release, effectively removing these neurons from the network. Alternatively, it is proposed that just a small subset of preBötC excitatory neurons may generate the inspiratory rhythm (*30*) and perhaps these key *Oprm1* neurons are enriched within this subgroup. In this instance, since hyperpolarization of preBötC rhythmogenic neurons slows and silences breathing (*31*), opioids may act postsynaptically as proposed by others (*7*,*32*). Regardless, it is profound that such a small number can abruptly halt the respiratory rhythm in a network of more than 1000 neurons and suggests that either these neurons act as a key population for rhythmogenesis, or that recurrent excitatory networks are exquisitely sensitive to the number of participating cells. Important future work will need to use the *Dbx1/Oprm1* and *Foxp2/Oprm1* molecular codes to selectively eliminate *Oprm1* from these neurons to test if truly so few neurons profoundly control or modulate breathing *in vivo*.

Methods

Animals

Oprm1$^{f/f}$ (*33*), *Oprm1*-mCherry (*34*), *Slc17a6*-Cre (*35*), *Gad2*-Cre (*36*), *Slc32a1*-Cre (*35*), *Slc6a5*-Cre (*37*), *Dbx1*-Cre (*38*), *Foxp2*-Cre (*39*), Rosa-LSL-YFP (*40*) have been described. Littermates of transgene-containing mice were used as wild type controls. C57Bl/6 mice were used for single cell mRNA sequencing. Mice were housed in a 12-hour light/dark cycle with unrestricted food and water. *Oprm1*$^{f/f}$ mice were assigned into experimental and control groups at weaning and given anonymized identities for experimentation and data collection. All animal experiments were performed in accordance with national and institutional guidelines with

standard precautions to minimize animal stress and the number of animals used in each experiment.

Recombinant viruses

All viral procedures followed the Biosafety Guidelines approved by the University of California, San Francisco (UCSF) Institutional Animal Care and Use Program (IACUC) and Institutional Biosafety Committee (IBC). The following viruses were used: AAV5-CMV-Cre-GFP ($4.7x10^{19}$ particles/mL, The Vector Core at the University of North Carolina at Chapel Hill), AAV5-CAG-GFP ($1.0x10^{13}$ particles/mL, The Vector Core at the University of North Carolina at Chapel Hill) or AAV5-CAG-tdtomato ($4.3x10^{12}$ particles/mL, The Vector Core at the University of North Carolina at Chapel Hill).

Immunostaining

Postnatal day 0-4 brains were dissected in cold PBS, and adult brains were perfused with cold PBS and then 4% paraformaldehyde by intracardiac perfusion. The isolated brains from neonates and adults were then fixed in 4% paraformaldehyde overnight at 4°C and dehydrated in 30% sucrose the next 24 hrs at 4°C. Brains were embedded and frozen in OCT once equilibrated in 30% sucrose. Cryosections (18-25 μM) were washed twice for 5 minutes in 0.1% Tween-20 in PBS, once for 10 minutes in 0.3% Triton-X100 in PBS, and then twice for 5 minutes in 0.1% Tween-20 in PBS. Following wash, sections were blocked for 20 minutes with either 10% goat serum in 0.3% Trition-X100 PBS. Sections were then incubated overnight at 4°C in the appropriate block solution containing primary antibody. Primary antibodies used were: rabbit anti-SST (Peninsula T-4103, 1:500), rabbit anti-FOXP2 (Abcam ab16046, 1:500), chicken anti-GFP (Abcam ab13970, 1:500), rat anti-mCherry (Lifetech. M11217, 1:500). After primary incubation, sections were washed three times for 10 minutes in 0.1% Tween-20 in PBS, then incubated for 1 hour at room temperature or overnight at 4°C in block containing secondary antibody. Secondary antibodies were: goat anti-rat 555 (Lifetech A21434, 1:200), goat anti-chicken 488 (Lifetech A11039, 1:200), goat anti-rabbit 633 (Lifetech 35562, 1:200). After

secondary incubation, sections were washed in 0.1% Tween-20 in PBS and mounted in Mowiol with DAPI mounting media to prevent photobleaching.

Plethysmography, respiratory and behavioral analysis

Adult (8-20 weeks) *Oprm1*$^{f/f}$ mice were first administered either IP 100-200µL of saline or morphine (20mg/kg, Henry Schein 057202) and placed in an isolated recovery cage for 15 minutes to allow full onset of action of the drug. Individual mice were then monitored in a 450 mL whole animal plethysmography chamber at room temperature (22°C) in 21% O_2 balanced with N_2 (normoxia) or 21% O_2, 5% CO_2 balanced with N_2 (hypercapnia). For fentanyl (150mg/kg, Sigma F3886) onset of action was so fast (<10sec) that animals were placed directly in the plethysmography chamber after administration of drug. Each session (combination of drug and oxygen condition) was separated by at least 24 hours to allow full recovery. Breathing was monitored by plethysmography, and other activity in the chamber monitored by video recording, for 40-minute periods in normoxia and 10-minute periods in hypercapnia. In cases where mice were subject to single or double site AAV injection to delete *Oprm1* or sham controls, breathing was recorded first before viral injection and then again after deletion (or sham) more than 4 weeks later. Breathing traces were collected using EMKA iOX2 software and exported to Matlab for analysis. Each breath was automatically segmented based on airflow crossing zero as well as quality control metrics. Respiratory parameters (e.g. peak inspiratory flow, instantaneous frequency, pause length, tidal volume, etc) for each breath, as well as averages across states, were then calculated. Instantaneous frequency was defined as the inverse of breath duration. Pause length was defined as the expiratory period after airflow dropped below 0.5 mL/sec. The pause period is initially a prolonged airflow around or just above 0 mL/sec. and terminates with an increase in expiratory airflow, likely the active expiration induced by hypercapnia (*11*, Fig. 2.5). The 0.5 mL/sec. threshold was chosen since it identifies low airflow pauses that are just above 0 mL/sec. which rarely occur in control hypercapnic breaths (Fig. 2.6). Prolonged pauses lasting 50-300msec. were only observed after morphine injection. Other respiratory parameters

were defined by when airflow crosses the value of 0, with positive to negative being inspiration onset and negative to positive being expiration onset. Note, reported airflow in mL/sec. and tidal volume in mL are approximates of the true volumes. Whole body plethysmography imperfectly measures these parameters without corrections for humidity and temperature. However, since humidity and temperature are largely stable between recordings, because they are conducted in a temperature and humidity stable mouse facility, the estimated airflow (mL/sec.) and tidal volume (mL) can be compared in saline vs. morphine or pre and post-Cre virus injection studies. Additionally, in some instances respiratory parameters are appropriately normalized to animal weight in order to accurately compare between animals. However, this normalization is not appropriate for our study since lung volume in mice does not change in adulthood (*41*), and all respiratory measurements are compared statistically as the ratio of saline to morphine injections within the same animal.

Due to limitations in breeding, a power calculation was not explicitly performed before our studies. Studies were conducted on all mice generated; six cohorts of animals. After respiration was measured, mice were sacrificed and injection sites were validated before inclusion of the data for further statistical analysis. We first conducted a Shapiro-Wilk normality on the average values (averaged across breaths) of the pre- and post-morphine respiratory parameters (e.g., peak inspiratory flow, instantaneous frequency) from n=29 animals. We then used either paired Student's t-test (if normal) or Wilcox Rank Sum test (if not normal) to evaluate statistical significance in comparing the distribution of these values. In comparisons of *Oprm1*-deleted vs. Sham conditions a mixed-repeated measure two-way ANOVA was performed to determine if these two groups were significantly different. Post-hoc Student's t or Wilcox Rank Sum tests were then used to evaluate statistical significance between normalized (morphine/saline, or morphine-saline) respiratory parameters for intact vs. *Oprm1* deleted or intact vs. Sham conditions. Normality in this case was determined by Shapiro-Wilk test on the distribution of normalized respiratory parameters from n=29 animals. All the above statistics

were performed using the publicly available Excel package “Real Statistics Functions” and SPSS.

Tail flick assays

Mice were injected with saline (control trials) or 20mg/kg morphine. 15-minutes later mice were put into a restraining wire mesh with the tail exposed. One-third of the tail was dipped into a 48-50°C water bath and time was measured for the tail to flick. Immediately after the flick, the tail was removed from the bath. If the tail did not flick within 10-seconds, then the tail was removed. The procedure was video recorded so time to response could be quantified post-hoc. Each mouse was recorded for two saline and two morphine trials.

Stereotaxic injection

Bilateral stereotaxic injections were performed in mice anaesthetized by isoflurane. Coordinates used for the preBötC were: -6.75 mm posterior, -5.05 mm ventral from surface, ±1.3 mm lateral from bregma. Coordinates used for the PBN/KF were: -5.05 mm posterior, -3.7 ventral from surface, ±1.7 lateral from bregma. Injection sites were confirmed by the restricted expression of Cre-GFP, GFP, or tdTomato in the anatomically defined Parabrachial/Kolliker-Fuse (*42*) and preBötC (*14,15*) areas. In the case of preBötC injections, anatomical location of injection site was also confirmed by localization with Somatostatin antibody staining (*43*). After injection of the virus, mice recovered for at least 3-4 weeks before breathing metrics were recorded again. In a subset of animals, mice were then subject to a second site deletion of the complementary brain area, ie. preBötC and then from the PBN/KF (Cohort 1) or vice versa (Cohort 2). These mice were then allowed to recover for another period of at least 3-4 weeks, after which a third set of breathing metrics were recorded. A subset of PBN/KF injected mice had only unilateral expression of Cre and their use is acknowledged in the text.

Slice electrophysiology

Rhythmic 550 to 650μm-thick transverse medullary slices which contain the preBötC and cranial nerve XII (XIIn) from neonatal *Oprm1*$^{f/f}$, *Oprm1*$^{f/f}$;*Slc17a6*-Cre+/-, *Oprm1*$^{f/f}$;*Gad2*-Cre+/-,

Oprm1$^{f/f}$;*Slc6a5*-Cre+/-, *Oprm1*$^{f/f}$;*Slc32a1*-Cre+/-, *Oprm1*$^{f/f}$;*Dbx1*-Cre+/-, *Oprm1*$^{f/f}$;*Foxp2*-Cre+/- (P0-5) were prepared as described (*44*). Briefly, slices were cut in ACSF containing (in mM): 124 NaCl, 3 KCl, 1.5 $CaCl_2$, 1 $MgSO_4$, 25 $NaHCO_3$, 0.5 NaH_2PO_4, and 30 D-glucose, equilibrated with 95% O_2 and 5% CO_2 (4°C, pH=7.4). The rostral portion of the slice was taken once the compact nucleus ambiguus was visualized. The dorsal side of each slice containing the closing of the 4th ventricle. For recordings, slices were incubated with ACSF from above and the extracellular K^+ was raised to 9 mM and temperature to 27°C. Slices equilibrated for 20 min before experiments were started. The preBötC neural activity was recorded from either XIIn rootlet or as population activity directly from the XII motor nucleus using suction electrodes. Activity was recorded with a MultiClamp700A or B using pClamp9 at 10000 Hz and low/high pass filtered at 3/400Hz. After equilibration, 20min. of baseline activity was collected and then increasing concentrations of DAMGO (ab120674) were bath applied (20nM, 50nM, 100nM, 500nM). Activity was recorded for 20min. after each DAMGO application. After the rhythm was eliminated or 500nM DAMGO was reached, 100nM Naloxone (Sigma Aldrich N7758) was bath applied to demonstrate slice viability. Rhythmic activity was normalized to the first control recording for dose response curves.

Single Cell mRNA Sequencing and analysis

650 µm-thick medullary slices containing the preBötC were prepared from 10 P0 mice C57Bl/6 mice as described above. The preBötC and surrounding tissue was punched out of each slice with a P200 pipette tip and incubated in bubbled ACSF containing 1mg/ml pronase for 30 minutes at 37°C with intermittent movement. Digested tissue was centrifuged at 800rpm for 1 minute, and the supernatant was discarded and replaced with 1% FBS in bubbled ACSF. The cell suspension was triturated serially with fire-polished pipettes with ~600µm, ~300µm and ~150µm diameter. The cells were filtered using a 40-µm cell strainer (Falcon 352340). DAPI was added to a final concentration of 1µg/mL. The cell suspension was FACS sorted on a BD

FACS AriaII for living (DAPI negative) single cells. The cells were centrifuged at 300g for 5 minutes and resuspended in 30 µL 0.04% BSA in PBS. The library was prepared using the 10x Genomics Chromium™ Single Cell 3' Library and Gel Bead Kit v2 (1206267) and according to manufacturer's instructions by the Gladstone genomics core. The final libraries were sequenced on HiSeq 4000.

For analysis, sequencing reads were processed using the 10x Genomics Cell Ranger v.2.01 pipeline. A total of 1860 cells were sequenced. Further analysis was performed using Seurat v2.3. Cells with less than 200 genes were removed from the dataset. Data was LogNormalized and scaled at 1e4. Highly variable genes were identified and used for principal component analysis. 25 principal components were used for unsupervised clustering using the FindCluster function. 12 clusters were identified at a resolution of 1.0, displayed in Fig. 2.14. FindAllMarkers and violin plots of known cell type markers were used to identify each cluster.

Figures

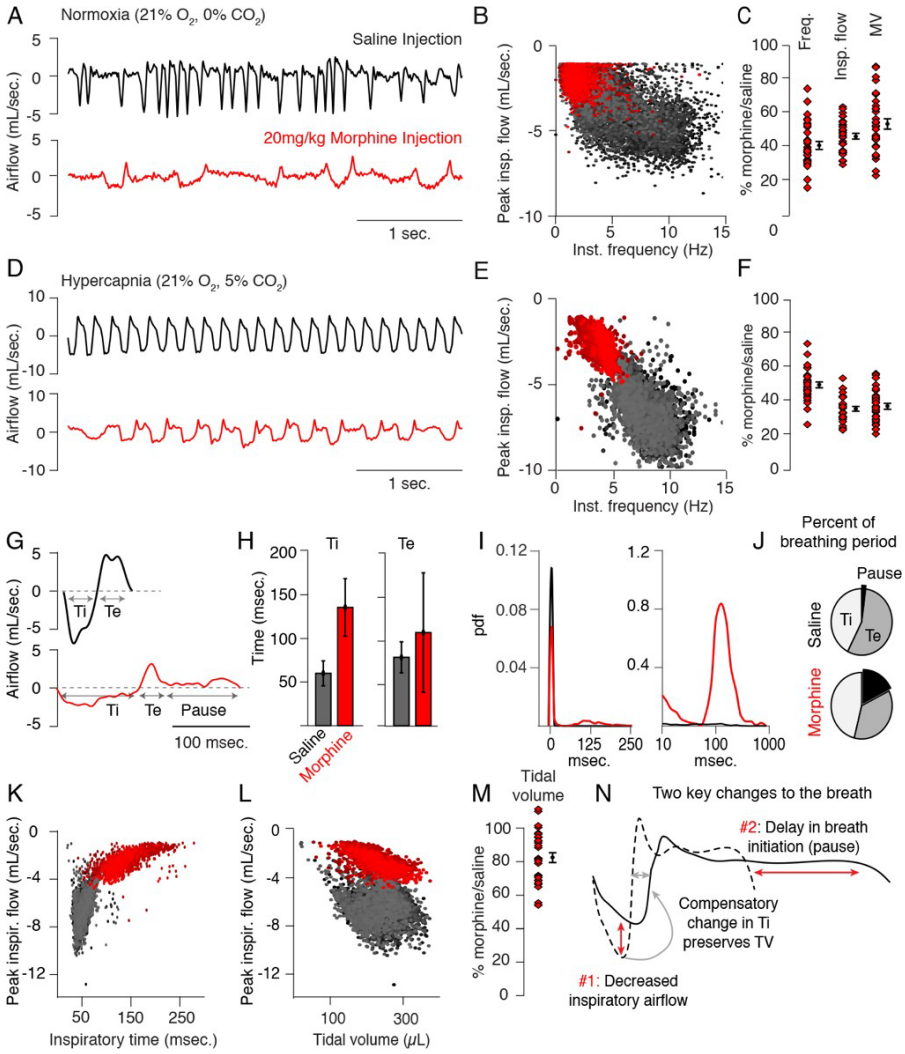

Fig. 2.1: Changes to breathing during opioid-induced respiratory depression. A, Representative examples of the breathing airflow (mL/sec.) in normoxia (21% O_2) measured by whole body plethysmography. 15 minutes before recordings, animals are intraperitoneally (IP) injected with either saline (black) or 20 mg/kg morphine (red). Morphine recordings are captured 1-7 days after saline. **B**, Scatterplot of instantaneous breathing rate (Hz) versus airflow (mL/sec.) for each breath (dot) taken during the 40-minute recordings. Morphine causes breathing to become slow and less forceful. **C**, Ratio of average breathing parameters after IP injection of morphine-to-saline. Respiratory rate, peak inspiratory airflow, and minute ventilation (MV= approximated tidal volume*rate) for n = 29 animals in normoxia. Red diamond, single animal average. Black diamond, average of all animals. Error bar, standard error of mean (SEM). **D-E**, Representative example of breathing airflow and instantaneous scatter plot (rate vs. airflow) from a 10-minute whole body plethysmography recording of breathing in hypercapnia (21% O_2, 5% CO_2) to minimize changes in breathing due to differences in behavior after morphine injection. **F**, Ratio of respiratory rate (p-value=$1x10^{-19}$, Cohen's d=5.96), peak inspiratory airflow (p-value=$1x10^{-22}$, Cohen's d=6.18), and minute ventilation (p-value=$1x10^{-20}$, Cohen's d=5.31) after IP injection of morphine-to-saline for n = 29 animals in hypercapnia. **G**,

Representative single breath airflow trace for breaths in hypercapnia after saline (black) or morphine (red) IP injection. Hypercapnic saline breaths can be divided into two phases whose durations (msec.) can be measured: inspiration (Ti) and expiration (Te). Hypercapnic morphine breaths have a third phase after expiration where airflow is nearly 0 mL/sec., which we call a pause. **H**, Bar graph of the average length ± standard deviation of Ti and Te for a single representative animal. **I,** Probability density function plot of the pause length in breathing during hypercapnia after saline (black) or morphine (red) IP injection on a numerical (left) and logarithmic scale (right). Note, morphine selectively increases Ti and pause length. **J**, Percent of the average breath period spent in inspiration, expiration, or pause for hypercapnic breaths after saline or morphine injection. **K**, Scatterplot of inspiratory time (msec.) vs. peak inspiratory airflow (mL/sec.) for 10-minutes of hypercapnic breaths after saline (black) or morphine (red) IP injection. As inspiratory time increases, peak inspiratory flow decreases. **L**, Scatterplot of tidal volume (μL.) vs. peak inspiratory airflow (mL/sec.) for 10-minutes of hypercapnic breaths after saline (black) or morphine (red) IP injection. Even though peak inspiratory airflow decreases after morphine, tidal volume is preserved due to prolonged Ti. **M**, Ratio of tidal volume after IP injection of morphine-to-saline for n = 29 animals in hypercapnia (p-value=$3x10^{-6}$, Cohen's d=1.13). **N**, Schematic of the two key morphine induced changes to the breath: decreased inspiratory airflow and pause. Decreased inspiratory airflow prolongs Ti since negative feedback from the lung reflecting breath volume is slower. We interpret the pause as a delay in initiation of the subsequent inspiration.

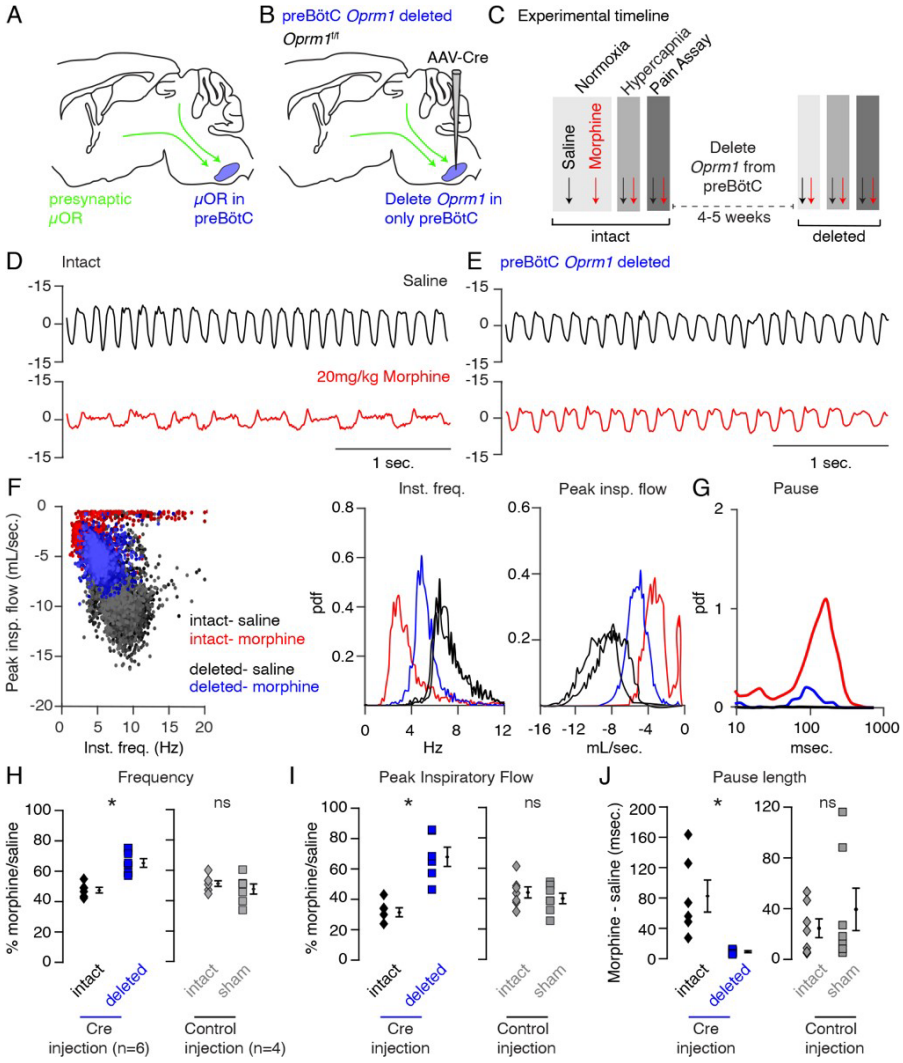

Fig. 2.2: Necessity of preBötC ventrolateral brainstem in opioid-induced respiratory depression. A, Schematic of a sagittal section through the adult mouse brain. The μ-Opioid receptor (*Oprm1*) is expressed by a subset of preBötC neurons and is also expressed on presynaptic terminals of some neurons projecting to the preBötC. This confounds the effects observed after localized preBötC injection of opioid or naloxone to investigate its role in OIRD. **B,** To overcome this, we eliminate *Oprm1* only from the preBötC, and not the presynaptic inputs, to define the role of preBötC neurons in OIRD. **C**, Experimental time-course. Breathing is measured 15-minutes after IP injection of saline or 20mg/kg morphine in both normoxia and hypercapnia. Then *Oprm1*$^{f/f}$ animals are injected with a constitutive-Cre AAV into the preBötC bilaterally. After several weeks breathing is assayed again as above. In this way, each animal's breathing before viral injection can serve as its own control breathing. Response to pain is also measured with a tail-flick assay before and after viral injection to ensure that analgesic response is unaffected. **D-E**, Representative examples of the breathing airflow (mL/sec.) in hypercapnia after saline (black) or morphine (red) before (**D**) and after (**E**) Cre-virus injection. **F,** Scatter plot of instantaneous respiratory frequency vs. airflow (ml/sec), as well as probability density function plots of both parameters for a representative animal during hypercapnia after saline (black) or morphine (red, blue) IP injection, before (red) and after (blue) Cre-injection. **G**, Probability density function plot of pause length (msec.) for a representative animal during

hypercapnia after IP morphine before (red) and after (blue) Cre-injection, log scale. Prevalence of long duration pauses is greatly reduced. **H-J**, Ratio of average breathing parameters after IP injection of morphine-to-saline. Respiratory rate (**H,** p-value= 0.003, Cohen's d=3.0), peak inspiratory airflow (**I,** p-value=0.0005, Cohen's d=3.01), and pause length (**J,** p-value=0.04, Cohen's d=2.0) for 6 *Oprm1*$^{f/f}$ animals with Cre-virus injected into the preBötC or 7 control animals with reporter-virus injected into the preBötC. All sham p-values were not significant (>0.09) and Cohen's D<0.6. For each experiment "intact" values are before viral injection, with "deleted" and "sham" values representing post viral injection conditions in experimental and control animals, respectively. Diamond and square, single animal average. Mixed repeated two-way ANOVA comparing Cre vs. Sham injected was statistically significant for respiratory rate ($F(1,11)=5.5$, p-value=0.04) and pause ($F(1,11)=6.2$, p-value=0.03), but not for peak inspiratory airflow ($F(1,11)=2.1$, p-value=0.17) Black diamond, average of all animals. Error bar, standard error of mean (SEM). * indicates p-value <0.05. ns indicates p-value >0.05.

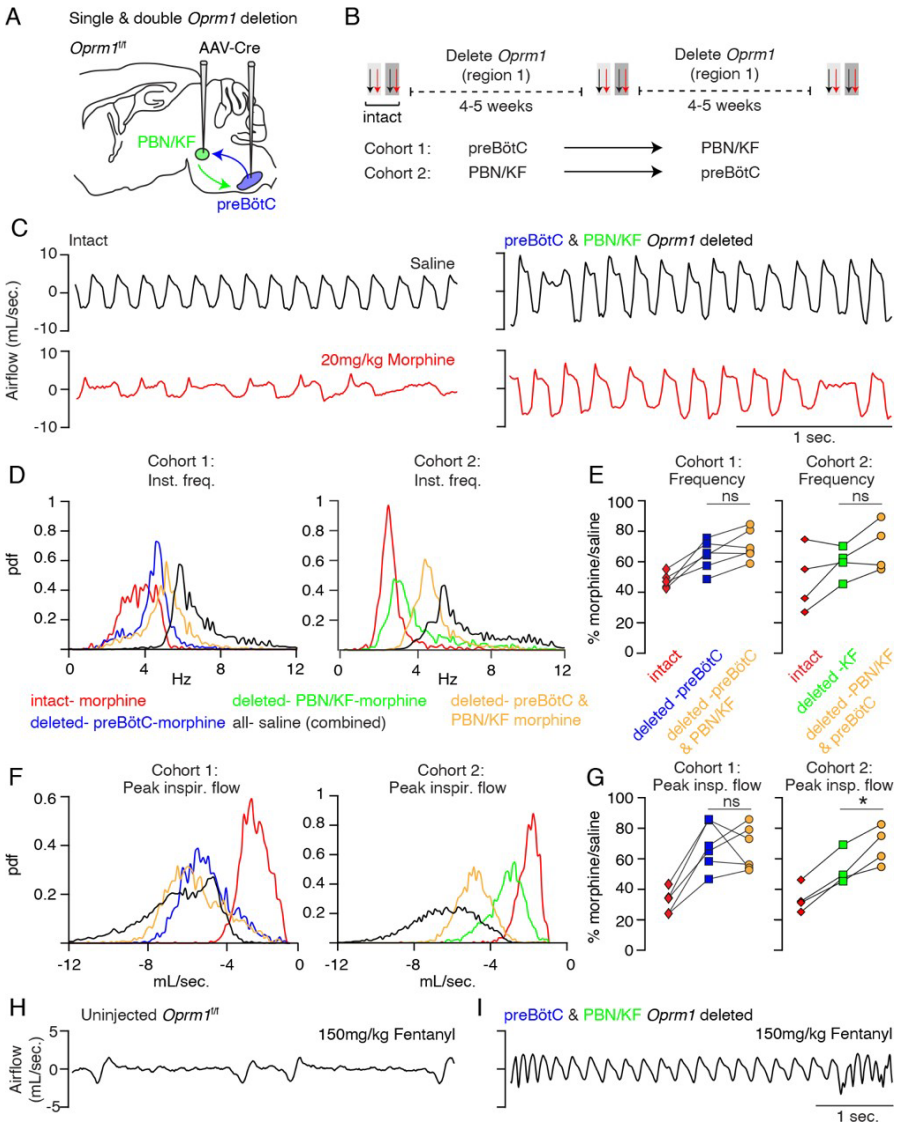

Fig. 2.3: Necessity of Parabrachial/Kolliker Fuse nuclei and preBötC in opioid-induced respiratory depression. A, Schematic of a sagittal section through the adult mouse brain showing Cre-viral injection into the preBötC and PBN/KF to measure their individual and combined contribution to OIRD. **B**, Like Fig. 2.2, breathing was assayed before and after each time Cre-virus was injected into *Oprm1$^{f/f}$* mice. In cohort 1, Cre-virus was first injected into the preBötC and then the PBN/KF and in cohort 2, Cre-virus was injected into the PBN/KF and then preBötC. **C**, Representative examples of the breathing airflow (mL/sec.) in hypercapnia for an animal in cohort 1 after saline (black) or morphine (red) before either viral injection and after both preBötC and PBN/KF Cre-virus injections. **D-E,** Probability density function plot of the instantaneous respiratory frequency for a representative animal from cohorts 1 and 2 (**D**) and ratio of average rate (**E**) after IP injection of morphine-to-saline for 6 animals in cohort 1 and 4 animals in cohort 2 before (pre) and after each Cre-virus injection into the preBötC (blue) or PBN/KF (green). Among the 2 cohorts, n=6 PBN/KF injections were bilateral and n=4 mostly unilateral. Cohort 1: preBötC vs. double p-value=0.07, Cohen's d=0.70. Cohort 2: PBN/KF vs. double p-value=0.1, Cohen's d=0.76. **F-G,** Probability density function plot of the peak inspiratory airflow for a representative animal from cohorts 1 and 2 (**F**) and ratio of average peak inspiratory airflow (**G**) after IP injection of morphine-to-saline before (pre) and after each Cre-

virus injection into the preBötC (blue) or PBN/KF (green). preBötC Cre-injection has a larger magnitude rescue and after preBötC and PBN/KF injections animals barely have any OIRD phenotype. Cohort 1: preBötC vs. double p-value=0.85, Cohen's d=0.10. Cohort 2: PBN/KF vs. double p-value=0.03, Cohen's d=1.32. **H-I,** Representative plethysmography traces in normoxia from a control *Oprm1*$^{f/f}$ mouse (N) or a double Cre-injected *Oprm1*$^{f/f}$ mouse (preBötC and PBN/KF, O) after IP injection of 150mg/kg fentanyl. * indicates p-value <0.05. ns indicates p-value >0.05.

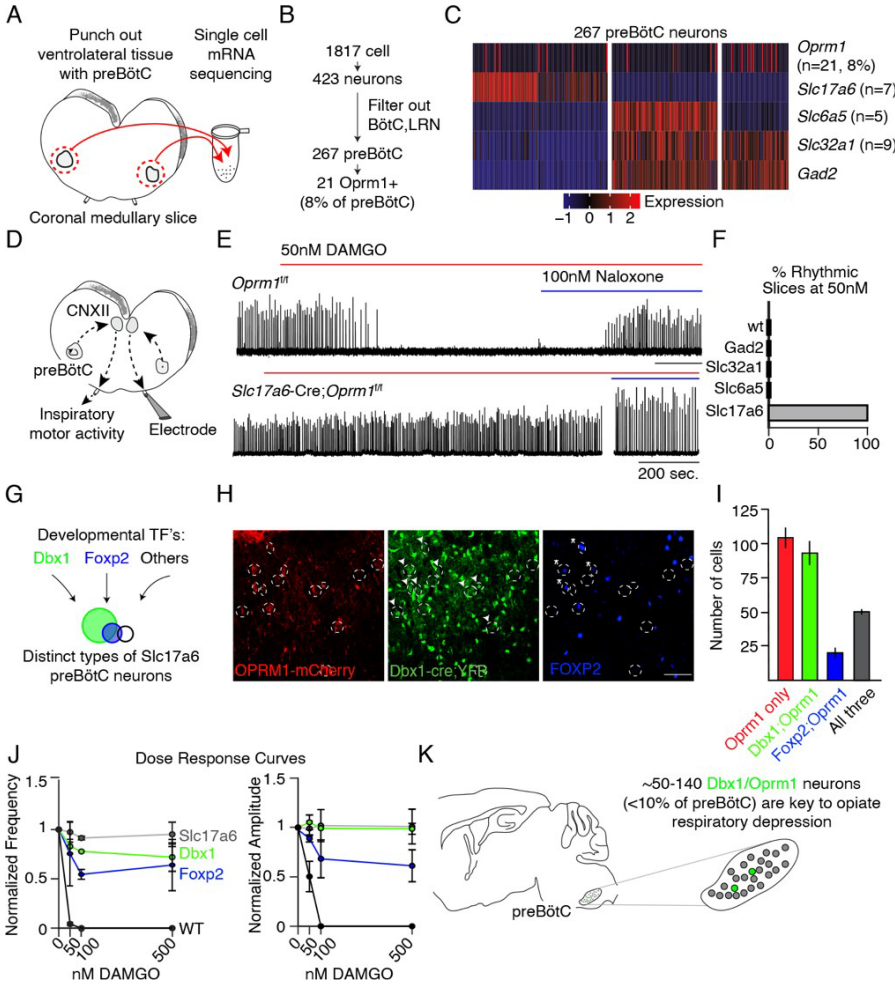

Fig. 2.4: Deletion of μ-Opioid receptor from neural subtypes to define their contribution to opioid depression of preBötC burst rhythm and amplitude. A, Schematic of single-cell mRNA sequencing paradigm. Postnatal day 0 (P0) medullary brainstem slices containing the preBötC bilaterally (circled in red) were dissected and isolated for sequencing. **B**, Single cell transcriptome profiling of cells isolated from P0 preBötC. Of 1817 cells isolated, only 267 were presumed preBötC neurons of which only 21 expressed *Oprm1* mRNA. **C**, Heatmap of scaled transcript abundance for *Oprm1* and markers of glutamatergic, gabaergic, and glycinergic preBötC neurons. *Oprm1* expressing cells are both excitatory and inhibitory. **D**, Schematic of extracellular recordings of the preBötC rhythm in P0-4 medullary brainstem slices. The preBötC has input to the hypoglossal motor neurons which form the CN12 rootlet, relaying an inspiratory motor command to the tongue in intact animals. Due to its input from the preBötC, extracellular recording from this rootlet display autonomous rhythmic activity corresponding to *in vitro* respiration (*5*). **E**, Representative recording of bursting activity after application of 50nM DAMGO and 100nM Naloxone. Top: in control (*Oprm1*$^{f/f}$) slices bath application of 50nM DAMGO quickly slowed and decreased the amplitude from baseline bursting. After rhythm cessation, bath application of Naloxone restored the rhythm. Bottom: in *Slc17a6*-cre*;Oprm1*$^{f/f}$ mice 50nM DAMGO did not stop, or even slow rhythmic activity. **F**, Percent of slices from each genotype with rhythm cessation after 50nM DAMGO application. Control (n=11), *Gad2*-Cre;*Oprm1*$^{f/f}$ (n=6), *Slc32a1*-Cre;*Oprm1*$^{f/f}$ (n=2), *Slc6a5*-Cre;*Oprm1*$^{f/f}$ (n=4), and *Slc17a6*-Cre;*Oprm1*$^{f/f}$ (n=3). **G**, Schematic showing three subpopulations of glutamatergic lineages delineated by transcription factors *Dbx1* and *Foxp2*. *Foxp2* neurons represents a smaller, and overlapping, population of *Dbx1* neurons. **H,** Identification of molecular subtypes of *Oprm1*

preBötC excitatory neurons. Sagittal section of the preBötC from a P0 *Oprm1*-mCherry;*Dbx1*-Cre;Rosa-LSL-YFP mouse immunostained for mCherry (OPRM1 fused to mCherry, red), YFP (Green) and FOXP2 (Blue). About ~50% of *Oprm1* preBötC neurons are glutamatergic/*Dbx1* derived (arrowhead) and of those, ~35% express FOXP2 (asterisk). Scale bar, 50μM. **I,** Quantification of the number of preBötC for each molecular subtype identified in **H**. **J**, Dose response curve for the bursting rate and amplitude after bath application of 0, 50, 100, and 500nM DAMGO applied to *Slc17a6*-Cre;*Oprm1*$^{f/f}$ (gray, n=3), *Dbx1*-Cre;*Oprm1*$^{f/f}$ (green, n=3), *Foxp2*-Cre;*Oprm1*$^{f/f}$ (blue, n=4) and control (black, n=11) P0-4 preBötC slices. Rate and amplitude for each slice are normalized to baseline. **K**, Schematic summary showing that the key node for opioids to suppress breathing is the preBötC and within this site, elimination of *Oprm1* from just a small subset of those neurons, ~70-140 excitatory neurons, prevents opioid respiratory suppression.

Tables

Table 1.1 Key Resources Table

Key Resources Table				
Reagent type (species) or resource		**Source or reference**	**Identifiers**	**Additional information**
Genetic reagent (*Mus musculus)*	*Oprm1*$^{f/f}$	The Jackson Laboratory	030074	RRID:IMSR_JAX:030074
Genetic reagent (*Mus musculus)*	*Oprm1*-mCherry	The Jackson Laboratory	029013	RRID:IMSR_JAX:29013
Genetic reagent (*Mus musculus)*	*Slc17a6*-Cre	The Jackson Laboratory	016963	RRID:IMSR_JAX:016963
Genetic reagent (*Mus musculus)*	*Gad2*-Cre	The Jackson Laboratory	0101802	RRID:IMSR_JAX:0101802
Genetic reagent (*Mus musculus)*	*Slc32a1-Cre*	The Jackson Laboratory	028862	RRID:IMSR_JAX:028862
Genetic reagent (*Mus musculus)*	*Slc6a5-Cre*	PMID:25643296		
Genetic reagent (*Mus musculus)*	*Dbx1*-Cre	PMID:16041369		
Genetic reagent (*Mus musculus)*	*Foxp2*-Cre	PMID:27210758		
Genetic reagent (*Mus musculus)*	Rosa-LSL-YFP	The Jackson Laboratory	006148	RRID:IMSR_JAX:006148
Adenovirus	AAV5-CMV-Cre-GFP	UNC Vector Core		AAV5
Adenovirus	AAV5-CAG-GFP	UNC Vector Core		AAV5

Reagent type (species) or resource		Source or reference	Identifiers	Additional information
Antibody	rabbit anti-SST	Peninsula	T-4103	1:500
Antibody	rabbit anti-FOXP2	Abcam	ab16046	1:500
Antibody	chicken anti-GFP	Abcam	ab13970	1:500
Antibody	rat anti-mCherry	Lifetech	M11217	1:500
Antibody	goat anti-rat 555	Lifetech	A21434	1:200
Antibody	goat anti-chicken 488	Lifetech	A11039	1:200
Antibody	goat anti-rabbit 633	Lifetech	35562	1:200
Chemical compound	Morphine sulfate	Henry Schein	057202	20mg/kg
Chemical compound	Fentanyl citrate	Sigma	F3886	150mg/kg
Peptide	DAMGO	Abcam	ab120674	20-500nM

Supplemental Figures

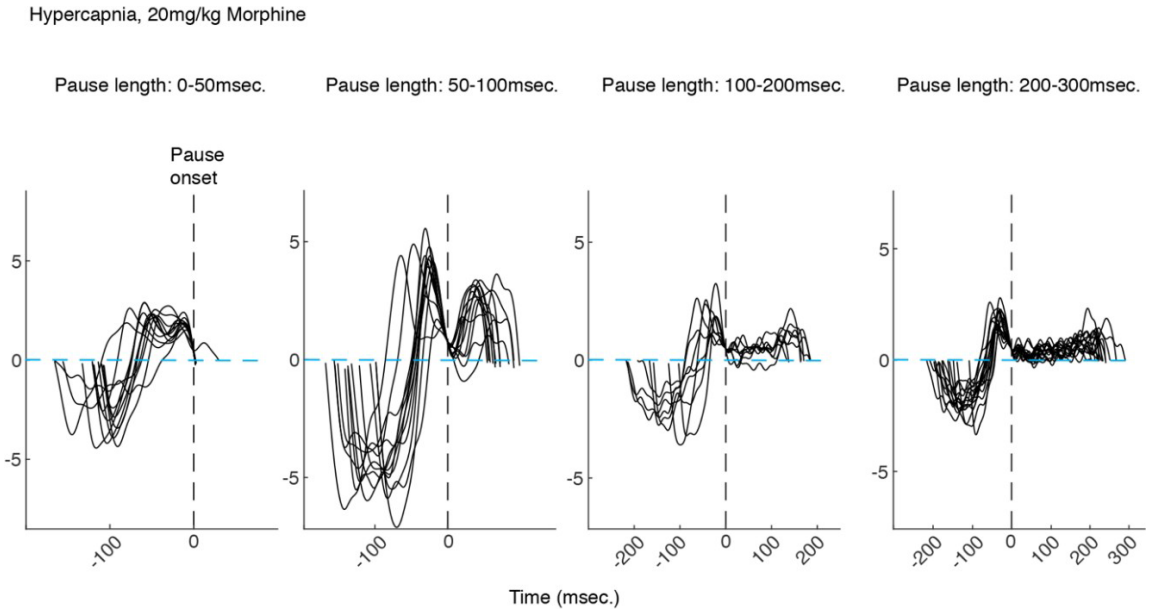

Fig. 2.5 (Figure 1- figure supplement 1): Examples of morphine breaths in hypercapnia binned by pause length. Example breaths binned by pause length (from left to right: 0-50, 50-100, 100-200, and 200-300msec.) from a control animal breathing in hypercapnia after intraperitoneal injection of 20mg/kg morphine. All breaths are aligned at the onset of the pause (vertical dashed black lines). Note that for longer pauses, the airflow is nearly 0 (dashed blue line) for tens to hundreds of milliseconds and then ends in an increased expiratory airflow, likely active expiration induced by hypercapnia.

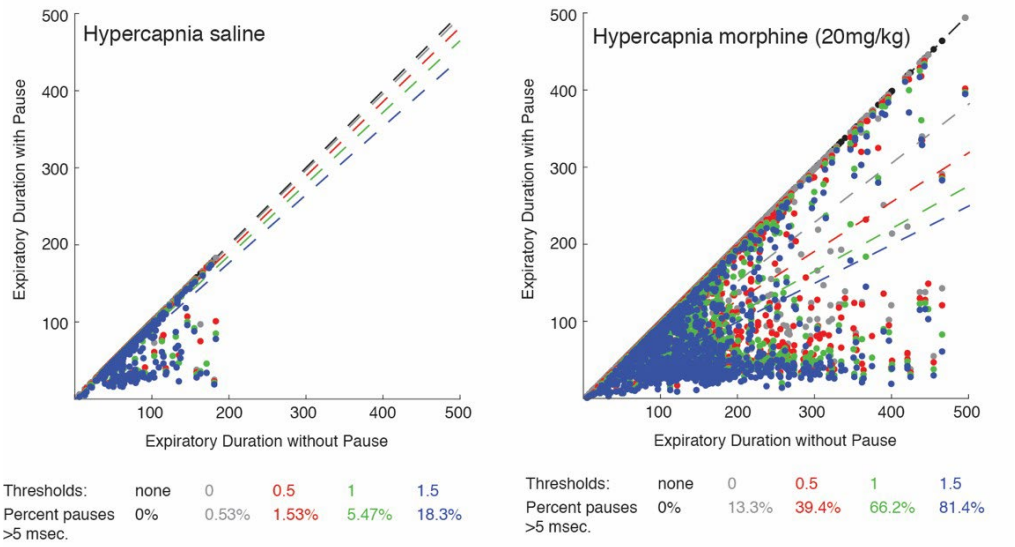

Fig. 2.6 (Figure 1- figure supplement 2): Scatter plot of expiratory duration with and without the pause to identify an effective airflow threshold. Scatterplots of 100 individual breaths (dots) from n=15 animals and the line of best fit (dashed line) where the expiratory length (msec.) of breaths is calculated with or without a pause. The different colors represent various airflow thresholds (mL/sec.) where the pause is initiated (black: no threshold, gray: 0mL/sec., red: 0.5mL/sec., green: 1mL/sec., blue: 1.5mL/sec.). Under hypercapnia conditions after intraperitoneal saline injection (left), at a pause threshold of 0.5mL/sec. less than 2% of all breaths had a pause defined greater than 5msec. However, after 20mg/kg morphine in hypercapnia, 40% of breaths had a pause greater than 5msec. At a threshold of 0.5mL/sec., since most breaths (>98%) under baseline conditions do not have any pause, this threshold was conservatively chosen for our analysis.

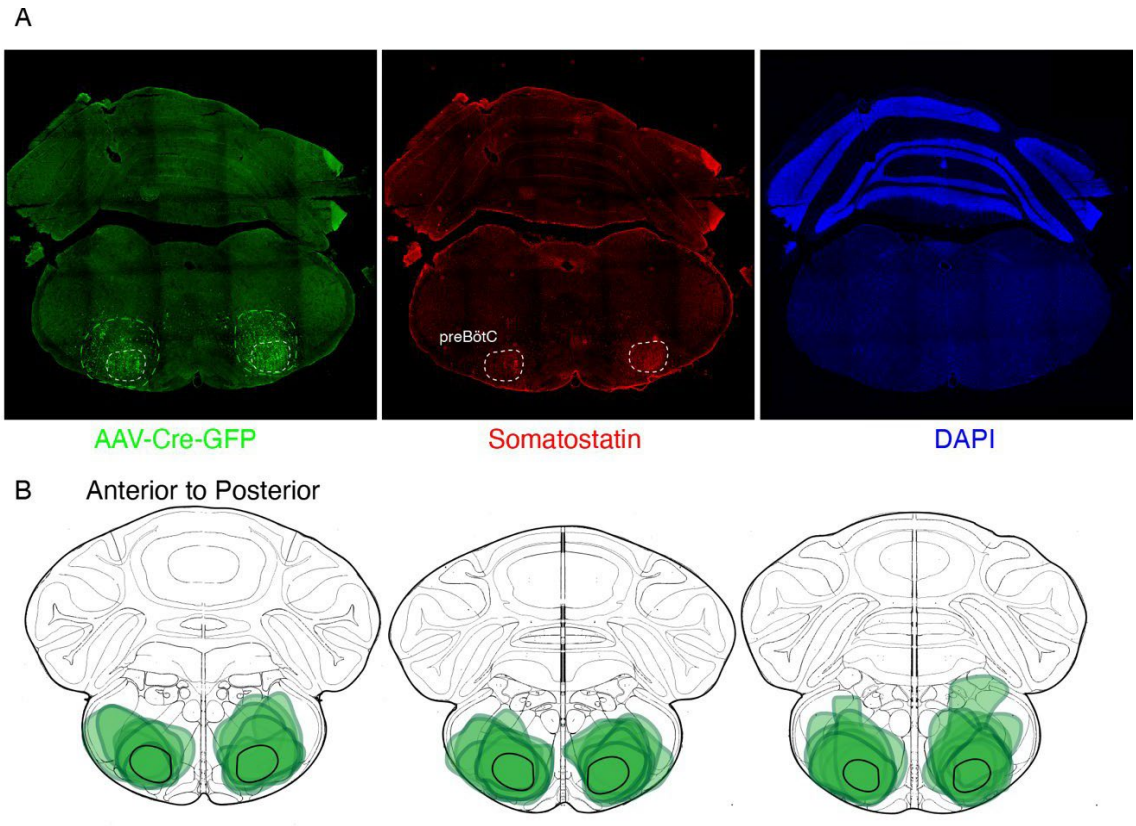

Fig. 2.7 (Figure 2 – figure supplement 1): Expression of GFP protein from AAV-Cre-GFP after bilateral preBötC injection. A, GFP protein (green) and Somatostatin neuropeptide (red) expression in a 25µM coronal section of the brainstem from an adult *Oprm1*$^{f/f}$ mouse injected bilaterally with AAV-Cre-GFP into the preBötC. Somatostatin expression demarcates the preBötC (dashed white circles, *43*). This validates the specific targeting of AAV-Cre, and thus *Oprm1* deletion, to the preBötC. **B**, Schematic of three serial coronal sections of the mouse brain from most anterior (left) to posterior (right) that cover the preBötC injection sites visualized by AAV-Cre-GFP expression (example in **A**). The extend of GFP expression for each injection site is highlighted by the green annotations in **B**, and the representative example in **A** (green dashed line). Note that overlap of all injection sites colocalizes with the preBötC (black solid line).

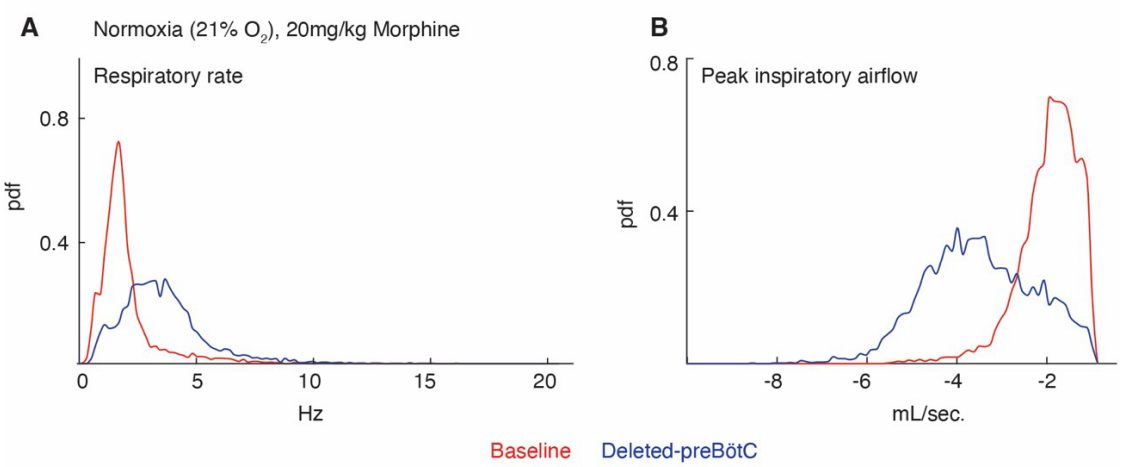

Fig. 2.8 (Figure 2 – figure supplement 2): Necessity of the preBötC for complete opioid induced respiratory depression in normoxia. The same animals in Figure 2.2 were also assayed for OIRD under normoxic instead of hypercapnic conditions. Briefly, breathing is measured 15-minutes after IP injection of 20mg/kg morphine in normoxia, animals are injected with a constitutive-Cre AAV into the preBötC bilaterally, and after several weeks re-assayed as above. **A-B**, A representative probability density function of respiratory rate (**A**) and peak inspiratory airflow (ml/sec, **B**) of all breaths taken during the 40-minute assay while in normoxia after intraperitoneal injection of 20mg/kg morphine before (red) and after (blue) AAV-Cre injection. The increased respiratory rate and peak inspiratory airflow after bilateral preBötC AAV-Cre injection indicates that the rescue of OIRD observed in hypercapnia also occurs in normoxia.

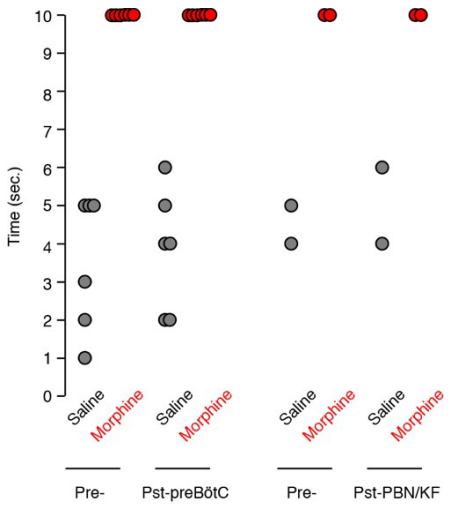

Fig. 2.9 (Figure 2 – figure supplement 3): Tail flick response before and after bilateral preBötC or PBN/KF injection. The tail flick response time was measured 15-minutes after IP saline (gray) or 20mg/kg morphine (red) injection. Each animal was assayed twice before (Pre-) and twice after (Pst-) bilateral AAV-Cre-GFP injection into either the preBötC or PBN/KF of adult *Oprm1*$^{f/f}$ mice. Dot, time for single assay of one animal. Note, *Oprm1* in the preBötC and PBN/KF is not required for morphine's ability to blunt the tail flick response.

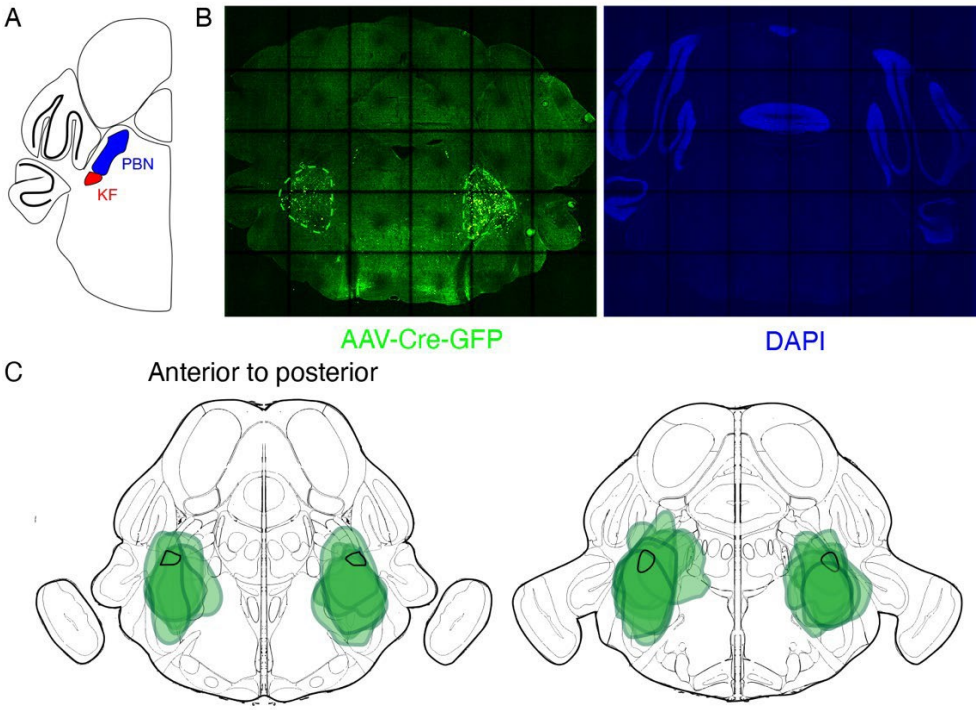

Fig. 2.10 (Figure 3 – figure supplement 1): Expression of GFP protein from AAV-Cre-GFP after bilateral PBN/KF injection. A, Schematic of a coronal section through the brainstem at the position of the PBN/KF. The PBN/KF is in the dorsal brainstem near the cerebellar peduncle. Half the brain is represented here. **B**, GFP protein (green) expression in a 25µM coronal section of the brainstem from an adult *Oprm1*$^{f/f}$ mouse injected bilaterally with AAV-Cre-GFP into the PBN/KF. This anatomical localization of GFP validates the specific targeting of AAV-Cre, and thus *Oprm1* deletion, to the PBN/KF. **C**, Schematic of two serial coronal sections of the mouse brain from most anterior (left) to posterior (right) that cover the PBN/KF injection sites visualized by AAV-Cre-GFP expression (example in **B**). The extend of GFP expression for each injection site is highlighted by the green annotations in **C**, and the representative example in **B** (green dashed line). Note that overlap of all injection sites contains the KF (black solid line).

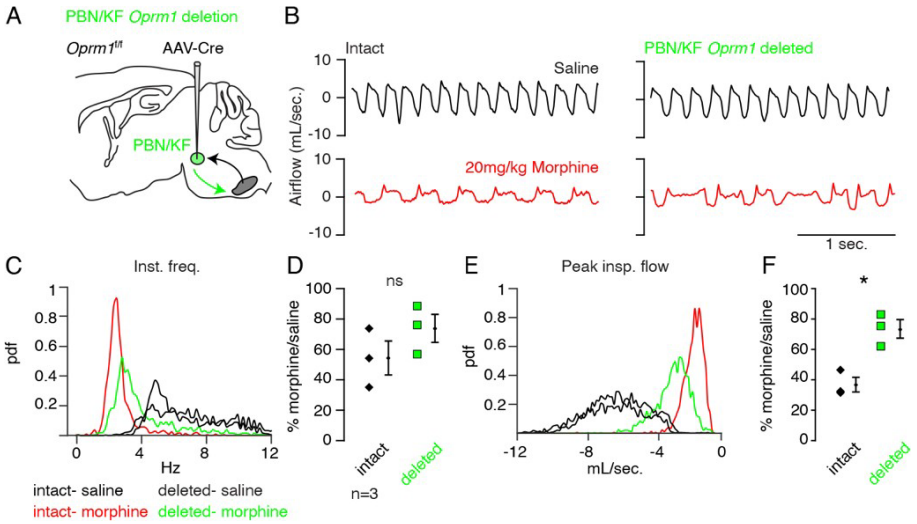

Fig. 2.11 (Figure 3 – figure supplement 2): Necessity of Parabrachial/Kolliker Fuse nuclei in opioid-induced respiratory depression. A, Schematic of a sagittal section through the adult mouse brain. *Oprm1* is expressed by neurons within the pontine Parabrachial/Kolliker Fuse (PBN/KF) which has modulatory input into the preBötC (*45,46*) and is a proposed region for respiratory depression during OIRD (*14,15*). As in Fig. 2.2, breathing was assayed before and after Cre-virus injection into the PBN/KF of *Oprm1*$^{f/f}$ mice. **B**, Representative examples of the breathing airflow (mL/sec.) in hypercapnia after saline (black) or morphine (red) before and after Cre-virus injection. **C-D,** Probability density function plot of the instantaneous respiratory frequency for a representative animal (**C**) and ratio of average rate (**D,** p-value=0.4, Cohen's d=0.62) after IP injection of morphine-to-saline for 3 animals before (pre) and after (post) Cre-virus injection into the PBN/KF. **E-F,** Probability density function plot of the peak inspiratory airflow for a representative animal (**E**) and ratio of average peak inspiratory airflow (**F,** p-value=0.02, Cohen's d=1.68) after IP injection of morphine-to-saline for 3 animals before (pre) and after (post) Cre-virus injection into the PBN/KF. * indicates p-value <0.05. ns indicates p-value >0.05.

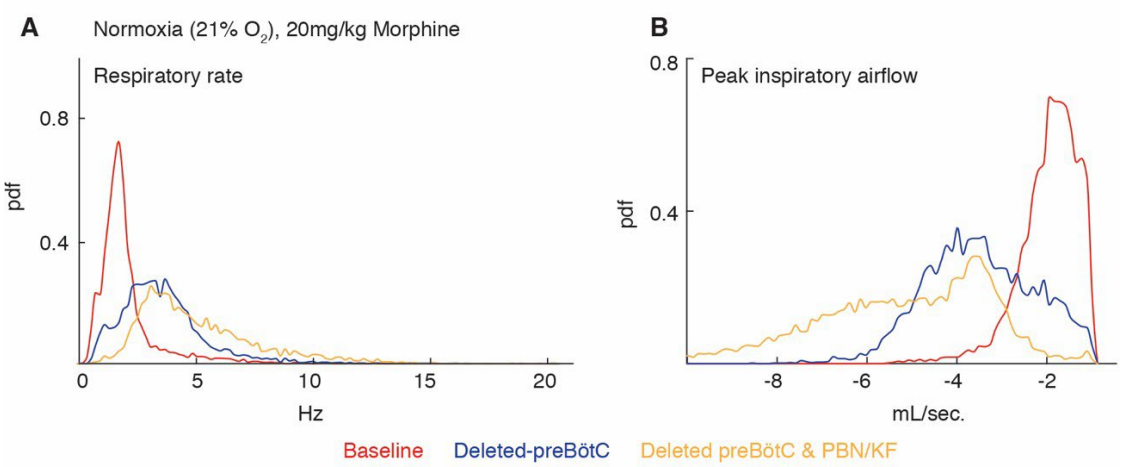

Fig 2.12 (Figure 3 – figure supplement 3): Necessity of the preBötC and PBN/KF for complete opioid induced respiratory depression in normoxia. The same animals in Figure 2.3 were also assayed for OIRD under normoxic instead of hypercapnic conditions. Breathing is measured 15-minutes after IP injection of 20mg/kg morphine in normoxia before, several weeks after animals are injected with a constitutive-Cre AAV into the preBötC or PBN/KF bilaterally, and then after the complementary brain site is injected. **A-B**, A representative probability density function of respiratory rate (**A**) and peak inspiratory airflow (ml/sec, **B**) of all breaths taken during the 40-minute assay while in normoxia after intraperitoneal injection of 20mg/kg morphine before (red), after AAV-Cre injection into the preBötC (blue), and after AAV-Cre injection into the PBN/KF (yellow). Note the slight increase in respiratory rate and peak inspiratory airflow after bilateral PBN/KF AAV-Cre injection is consistent with data collected in hypercapnia and indicates that the preBötC is the dominant site.

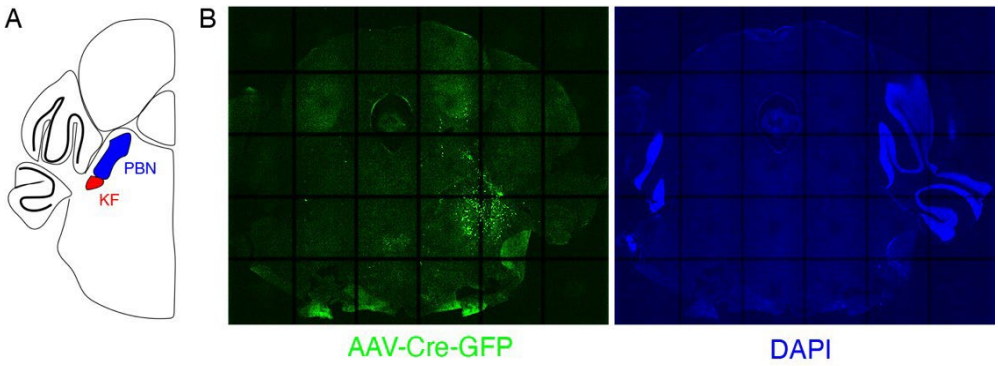

Fig. 2.13 (Figure 3 – figure supplement 4): Expression of GFP protein from AAV-Cre-GFP after mostly unilateral PBN/KF injection. A, Schematic of a coronal section through the brainstem at the position of the PBN/KF. The PBN/KF is in the dorsal brainstem near the cerebellar peduncle. Half the brain is represented here. **B**, GFP protein (green) expression in a 25μM coronal section of the brainstem from an adult *Oprm1*$^{f/f}$ mouse injected bilaterally with AAV-Cre-GFP into the PBN/KF. In this instance, GFP expression is robustly seen on right side and few cells are labeled on the left. This localization of GFP suggests targeting of AAV-Cre, and thus *Oprm1* deletion, is only in to one PBN/KF.

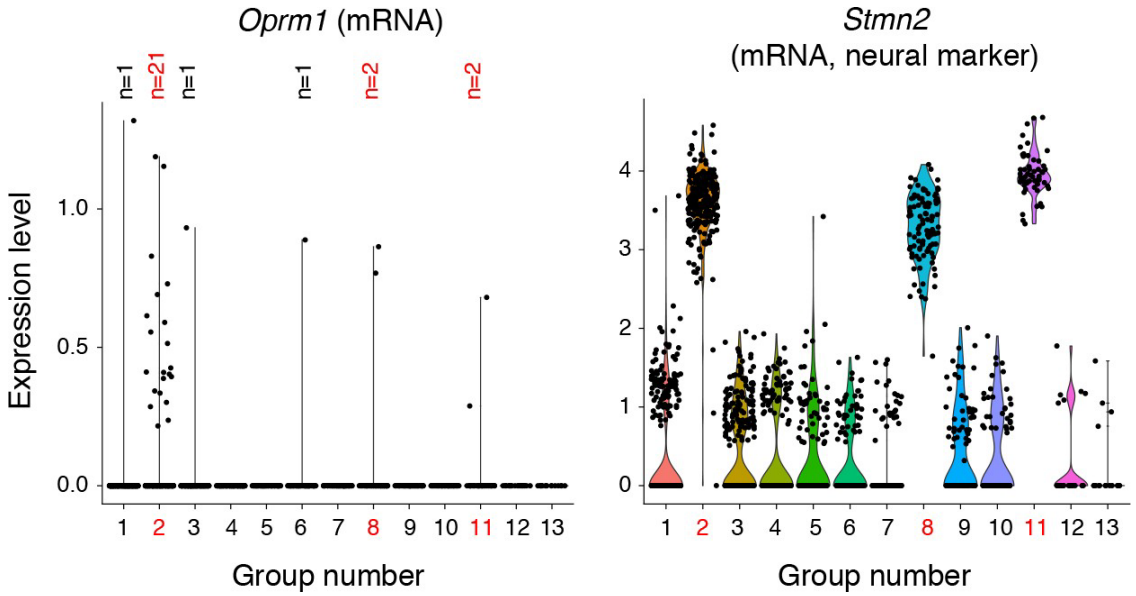

Fig. 2.14 (Figure 4 – figure supplement 1): Single cell transcriptome profiling of ventrolateral brainstem neurons. 1817 single cells were isolated from the ventrolateral medulla of the P0 mouse. The transcriptome was sequenced with 10X genomics technology and cells were clustered by principle components analysis into 13 groups. 3 groups (2, 8, and 11, red numbers) expressed neural markers like *Stmn2* (mRNA) shown here. Group 2 was a mixture of excitatory and inhibitory neurons and is the presumed preBötC cluster due to expression of *Sst*, *Tacr1*, and *Cdh9* (mRNA, not shown). Group 8 is a BötC cluster based on expression of *Gad1* and *Neurod6* (mRNA, not shown). Group 11 is a lateral reticular nucleus cluster based on expression of *Zic1* and *Barhl1* (mRNA, not shown). All other groups were oligodendrocytes, oligodendrocyte precursor cells, astrocytes, microglia and endothelial cells. The only group with enriched *Oprm1* (mRNA) expression is the preBötC group 2. Within this group only 21/267 neurons express *Oprm1* (mRNA). The single cell in group 1, 3, 6 (which are non-neural) that express *Oprm1* (mRNA) are presumed contaminants.

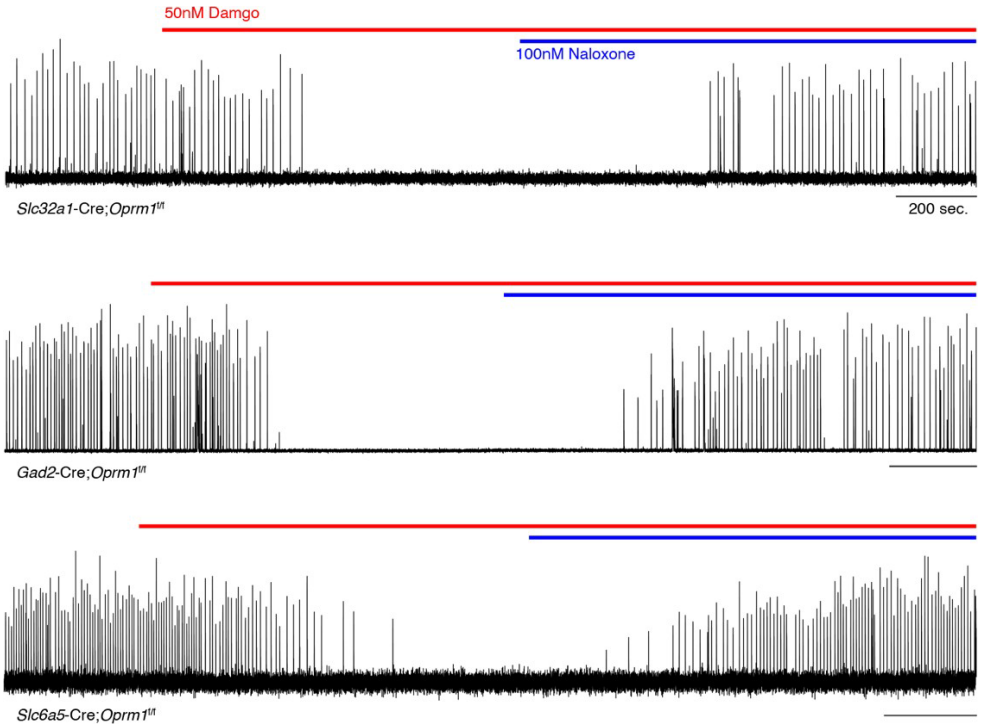

Fig. 2.15 (Figure 4 – figure supplement 2): preBötC slice activity in 50nM DAMGO after deletion of *Oprm1* from inhibitory neural types. Representative recording of bursting activity at baseline, after application of 50nM DAMGO (red line), and 100nM Naloxone (blue line). Top: *Slc32a1*-Cre;*Oprm1*$^{f/f}$ targeting GABAergic neurons (n=2). Middle: *Gad2*-Cre;*Oprm1*$^{f/f}$ targeting GABAergic neurons (n=6). Bottom: *Slc6a5*-Cre;*Oprm1*$^{f/f}$ targeting Glycinergic neurons (n=4).

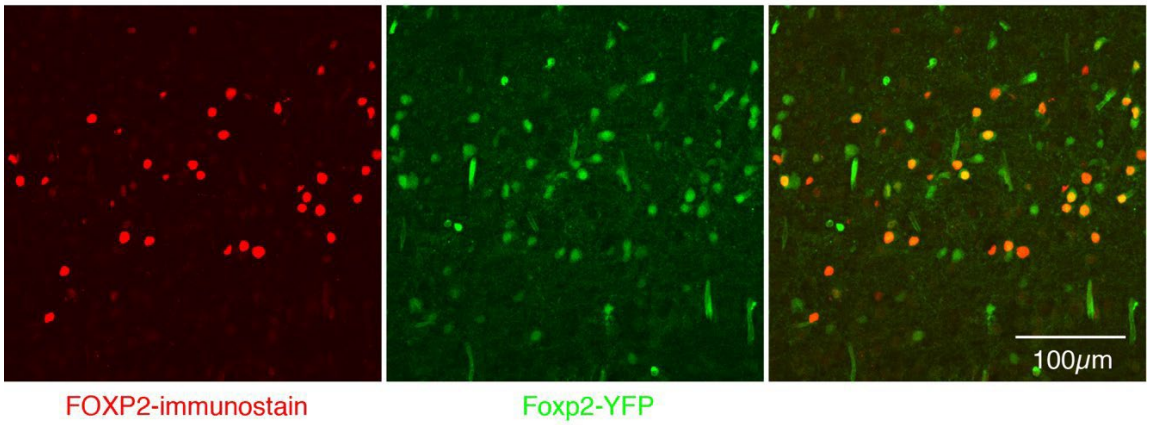

Fig. 2.16 (Figure 4 – figure supplement 3): Expression of FOXP2 protein and in Foxp2-derived cells within the preBötC. Nearly perfect colocalization of FOXP2 protein (red) and YFP (green) in a 25μM sagittal section of the preBötC from a P0 *Foxp2*-Cre;Rosa-LSL-YFP mouse. This validates the use of *Foxp2*-Cre to remove *Oprm1* from Foxp2-derived neurons. Scale bar, 100μM.

References

1. L. Scholl, P. Seth, M. Kariisa, N. Wilson, G. Baldwin, “Drug and Opioid-Involved Overdose Deaths – United States, 2013-2017”. WR Morb Mortal Wkly Rep. 67:1419-1427 (2018).
2. R.A. Rudd, N. Aleshire, J.E. Zibbell, R.M. Gladden, “Increases in Drug and Opioid Overdose Deaths – United States, 2000-2014”. MMWR. 64(50); 1378-82 (2016).
3. K.T. Pattinson, Opioids and the control of respiration. *Br J Anaesth.* ***6****,* 747-758 (2008).
4. A. Dahan, E. Sarton, L. Teppema, C. Olievier, D. Nieuwenhuijs, H.W. Matthes, B.L. Kieffer, Anesthetic potency and influence of morphine and sevoflurane on respiration in mu-opioid receptor knockout mice. *Anesthesiology*, ***94***, 824-832 (2001).
5. A. Mansour, C.A. Fox, S. Burke, F. Meng, R.C. Thompson, H. Akil, S.J Watson, Mu, delta, and kappa opioid receptor mRNA expression in the rat CNS: an in situ hybridization study. *Journal of Comparative Neurology*, ***350***, 412-438 (1994)
6. G.C. Kirby, D.S. McQueen, Characterization of opioid receptors in the cat carotid body involved in chemosensory depression in vivo. *British journal of pharmacology*, ***88,*** 889-898 (1986).
7. G. Montandon, W. Qin, H. Liu, J. Ren, J.J. Greer, R.L. Horner, PreBotzinger complex neurokinin-1 receptor-expressing neurons mediate opioid-induced respiratory depression. *J Neurosci.,* ***31***, 1292-1301 (2011).
8. S. Mustapic, T. Radocaj, A. Sanchez, Z. Dogas, A.G. Stucke, F.A. Hopp, E.A. Stuth, E.J. Zuperku, Clinically relevant infusion rates of mu-opioid agonist remifentanil cause bradypnea in decerebrate dogs but not via direct effects in the pre-Bötzinger complex region. *J Neurophysiol.*, ***103***, 409-418 (2010).
9. I. Prkic, S. Mustapic, T. Radocaj, A.G. Stucke, E.A. Stuth, F.A. Hopp, C. Dean, E.J. Zuperku, Pontine μ-opioid receptors mediate bradypnea caused by intravenous remifentanil infusions at clinically relevant concentrations in dogs. *J Neurophysiol.,* ***108***, 2430-2441 (2012).

10. A.G. Varga, B.T. Reid, B.L. Kieffer, E.S. Levitt, Differential impact of two critical respiratory centres in opioid-induced respiratory depression in awake mice. *J Physiol.* (2019).
11. A. Pisanski and S. Pagliardini. The parafacial respiratory group and the control of active expiration. *Resp. Phys. Neurobiol*. ***265***,153-160, 2019
12. J. F. West, *Respiratory physiology: the essentials*. (Lippincott Williams & Wilkins, Hagerstown, MD, 2005).
13. R. Hill, A. Disney, A. Conibear, K. Sutcliffe, W. Dewey, S. Husbands, C. Bailey, E. Kelly, G. Henderson, The novel μ-opioid receptor agonist PZM21 depresses respiration and induces tolerance to antinociception. *Br J Pharmacol., **175**,* 2653-2661 (2018).
14. J.C. Smith, H.H. Ellenberger, K. Ballanyi, D.W. Richter, J.L. Feldman, Pre-Bötzinger complex: a brainstem region that may generate respiratory rhythm in mammals. *Science*, ***254***, 726-729 (1991).
15. J.L. Feldman, C.A. Del Negro, P.A. Gray, Understanding to rhythm of breathing: so near, yet so far. *Annu Rev Physiol., **75***, 423-452 (2013).
16. Y. Cui, K. Kam, D. Sherman, W.A. Janczewski, Y. Zheng, J.L. Feldman, Defining preBötzinger complex rhythm- and pattern-generating neural microcircuits in vivo. *Neuron, **91***, 602-614 (2016).
17. G. Montandon, R. Horner, CrossTalk proposal: The preBotzinger complex is essential for the respiratory depression following systemic administration of opioid analgesics. *J Physiol,* **592**, 1159-1162 (2014).
18. A.W. Mudge, S.E. Leeman, G.D. Fischbach, Enkephalin inhibits release of substance P from sensory neurons in culture and decreases action potential duration. *Proc Natl Acad Sci U S A*, ***76***, 526-530 (1979).
19. E.G. Dobbins, J.L. Feldman, Brainstem network controlling descending drive to phrenic motoneurons in rat. *J Comp Neurol.*, ***347***, 64-86 (1994).

20. P.A. Gray, J.C. Rekling, C.M. Bocchiaro, J.L. Feldman, Modulation of respiratory frequency by peptidergic input to rhythmogenic neurons in the preBötzinger complex. *Science*, ***286*** 1566-1568 (1999).
21. K. Eguchi, E. Tadaki, D. Jr. Simbulan, T. Kumazawa, Respiratory depression caused by either morphine microinjection or repetitive electrical stimulation in the region of the nucleus parabrachialis of cats. *Pflugers Arch*., ***409***, 367-373 (1987).
22. P.M. Lalley, P.M. Pilowsky, H.V. Forster, E.J. Zuperku, CrossTalk opposing view: The preBotzinger complex is essential for the respiratory depression following systemic administration of opioid analgesics. *J Physiol,* **592**, 1163-1166 (2014).
23. A.R. Lorier, G.D. Funk, J.J. Greer, Opiate-induced suppression of rat hypoglossal motoneuron activity and its reversal by ampakine therapy. *PLoS One, **5***, e8766 (2010).
24. P.A. Gray, J.A. Hayes, G.Y. Ling, I. Llona, S. Tupal, M.C. Picardo, S.E. Ross, T. Hirata, J.G. Corbin, J. Eugenin, C.A. Del Negro, Developmental origin of preBötzinger complex respiratory neurons. *J Neurosci., **30**,* 14883-14895 (2010).
25. J. Bouvier, M. Thoby-Brisson, N. Renier, V. Dubreuil, J. Ericson, J. Champagnat, A. Pierani, A. Chedotal, G. Fortin, Hindbrain interneurons and axon guidance signaling critical for breathing. *Nat Neurosci., **13***, 1066-1074 (2010).
26. P.A. Gray, Transcription factors define the neuroanatomical organization of the medullary reticular formation. *Front Neuroanat.,* doi: 10.3389/fnana.2013.00007 (2013).
27. T. Manzke, U. Guenther, E.G. Ponimaskin, M. Haller, M. Dutschmann, S. Schwarzacher, D.W. Richter, 5-HT4(a) receptors avert opioid-induced breathing depression without loss of analgesia. *Science*, ***301***, 226-229 (2003).
28. R.T. Huckstepp, L.E. Henderson, K.P. Cardoza, J.L. Feldman, Interactions between respiratory oscillators in adult rats. *Elife*, ***5***, e14203 (2016).
29. X. Wang, J.A. Hayes, A.L. Revill, H. Song, A. Kottick, N.C. Vann, M.D. LaMar, M.C. Picardo, V.T. Akins, G.D. Funk, C.A. Del Negro, Laser ablation of Dbx1 neurons in the pre-Bötzinger

complex stops inspiratory rhythm and impairs output in neonatal mice. *Elife, **3***, e03427 (2014).

30. R.S. Phillips, T.T. John, H. Koizumi, Y.I. Molkov, J.C. Smith, Biophysical mechanisms in the mammalian respiratory oscillator re-examined with a new data-driven computational model. *Elife*, ***8***, e41555 (2019).
31. H. Koizumi, B. Mosher, T.F. Mohammad, R. Zhang, N. Koshiya, J.C. Smith, Voltage-dependent rhythmogenic property of respiratory pre-Bötzinger complex glutamatergic, Dbx1-derived, and somatostatin-expressing neuron populations revealed by graded optogenetic inhibition. *eNeuro*, ***3***, ENEURO.0081-16.2016 (2016).
32. S.M. Johnson, J.C. Smith, J.L. Feldman, Modulation of respiratory rhythm in vitro: Gi/o protein-mediated mechanisms. *J Appl. Physiol., **80***, 2120-2133 (1996).
33. R. Weibel, D. Reiss, L. Karchewski, O. Gardon, A. Matifas, D. Filliol, J.A. Becker, J.N. Wood, B.L. Kieffer, C. Gaveriaux-Ruff, Mu opioid receptors on primary afferent nav1.8 neurons contribute to opiate-induced analgesia: insight from conditional knockout mice. *PLoS One, **8***, e74706 (2013).
34. E. Erbs, L. Faget, G. Scherrer, A. Matifas, D. Filliol, J.L. Vonesch, M. Koch, P. Kessler, D. Hentsch, M.C. Birling, M. Koutsourakis, L. Vasseur, P. Veinante, B.L. Kieffer, D. Massotte, A mu-delta opioid receptor brain atlas reveals neuronal co-occurrence in subcortical networks. *Brain Struct Funct, **220***, 677-702 (2015).
35. L. Vong, C. Ye, Z. Yang, B. Choi, S. Jr. Chua, B.B. Lowell, Leptin Action on GABAergic Neurons Prevents Obesity and Reduces Inhibitory Tone to POMC Neurons. *Neuron, **71,*** 142-154 (2011).
36. H. Taniguchim, M. He, P. Wu, S. Kim, R. Paik, K. Sugino, D. Kvitsani, Y. Fu, J. Lu, Y. Lin, G. Miyoshi, Y. Shima, G. Fishell, S.B. Nelson, Z.J. Huang, A resource of cre driver lines for genetic targeting of GABAergic neurons in cerebral cortex. *Neuron, **71***, 995-1013 (2011).

37. D. Sherman, J.W. Worrell, Y. Cui, J.L. Feldman, Optogenetic perturbation of preBötzinger Complex inhibitory neurons modulates respiratory pattern. *Nat Neurosci., **18***, 408-414 (2015).

38. F. Bielle, A. Griveau, N. Narboux-Neme, S. Vigneau, M. Sigrist, S. Arber, M. Wassef, A. Peirani, Multiple origins of Cajal-Retzius cells at the borders of the developing pallium. *Nature Neuroscience. **8***, 1002-1012 (2005).

39. D.L Rousso, M. Qiao, R.D. Kagan, M. Yamagata, R.D. Palmiter, J.R. Sanes, Two Pairs of ON and OFF Retinal Ganglion Cells Are Defined by Intersectional Patterns of Transcription Factor Expression. *Cell Rep, **15***, 1930-1944 (2016).

40. L. Madisen, T.A. Zwingman, S.M. Sunkin, S.W. Oh, H.A. Zariwala, H. Gu, L.L. Ng, R.D. Palmiter, M.J. Hawrylycz, A.R. Jones, E.S. Lein, H. Zeng H, A robust and high-throughput Cre reporting and characterization system for the whole mouse brain. *Nat Neurosci., **13***, 133-140 (2010).

41. W. Mitzner, R. Brown, W. Lee, In vivo measurement of lung volumes in mice. *Physiol. Genomics, **4**,* 215-221 (2001).

42. E.S. Levitt, A.P. Abdala, J.F. Paton, J.M. Bissonnette, J.T. Williams, μ opioid receptor activation hyperpolarizes respiratory-controlling Kölliker-Fuse neurons and suppresses post-inspiratory drive. *J Physiol., **593***, 4453-4469 (2015).

43. W. Tan, W.A. Janczewski, P. Wang, X.M. Shao, E.M. Callaway, J.L. Feldman, Silencing preBötzinger complex somatostatin-expressing neurons induces persistent apnea in awake rat. *Nat Neurosci., **11***, 538-540 (2008).

44. A. Ruangkittisakul, A. Kottick, M.C. Picardo, K. Ballanyi, C.A. Del Negro, Identification of the pre-Bötzinger complex inspiratory center in calibrated “sandwich” slices from newborn mice with fluorescent Dbx1 interneurons. *Physiol. Rep., **2***, e12111 (2014).

45. N.L. Chamberlin, C.B. Saper, Topographic organization of respiratory responses to glutamate microstimulation of the parabrachial nucleus in the rat. *J Neurosci., **14***, 6500-6510 (1994).
46. G.F Alheid, W.K. Milsom, D.R. McCrimmon, Pontine influences on breathing: an overview. *Respir Physiol Neurobiol, **143*,** 105–114 (2004).

Chapter 3:

ß-arrestin 2 germline knockout does not attenuate opioid respiratory depression

---

Introduction

More than 180 people died each day in 2018 from depressed breathing following an opioid overdose, a lethal side-effect termed opioid induced respiratory depression (OIRD) (Pattinson, 2008; Scholl et al., 2018). Nevertheless, opioids remain among the most effective and widely prescribed analgesics, as evidenced by the World Health Organization's step ladder for pain management. These two contrasting characteristics have created the urgent desire to develop or discover novel μ-opioid receptor (MOR) agonists that provide analgesia without depressing breathing. Such a possibility emerged in 2005 when it was reported that mice with germline deletion of ß2-arrestin (*Arrb2-/-*) experience enhanced analgesia with attenuated respiratory depression when administered systemic morphine (Raehal et al., 2005). This finding inspired a new field of 'biased agonist' pharmacology with the goal of engaging MOR dependent G-protein but not ß2-arrestin signaling. This approach remains a central strategy in drug discovery for analgesics (Turnaturi et al., 2019).

Germline deletion of the μ-opioid receptor gene (*Oprm1*) completely eliminates OIRD in murine models (Dahan et al., 2001) and selective deletion of *Oprm1* within the brainstem medullary breathing rhythm generator, the preBötzinger Complex (preBötC) (Smith et al., 1991), largely attenuates OIRD (Bachmutsky et al., 2020; Varga et al., 2019). When engaged, MOR G-protein signaling activates inwardly rectifying potassium channels (Al-Hasani and Bruchas, 2011) and inhibits synaptic vesicle release (Zurawski et al., 2019), thereby depressing neural signaling. Additionally, the MOR signals intracellularly via a pathway dependent on MOR internalization by ß2-arrestin (Calebiro et al., 2010; Luttrell and Lefkowitz, 2002). Indeed, all three pathways have

been implicated in OIRD (Montandon et al., 2016; Raehal et al., 2005; Wei and Ramirez, 2019) but a role for *Arrb2* has been suggested to be important and selective for respiratory depression, relative to analgesia.

Since the original OIRD study of *Arrb2*-/- mice, multiple MOR agonists, dubbed 'biased agonists', have been created that signal through G-protein but not ß2-arrestin pathways. These agonists are reported to produce analgesia with reduced respiratory depression (Manglik et al., 2016; Schmid et al., 2017) and thereby provide pharmacological support for the proposed role of ß2-arrestin in OIRD. However, recently, these studies have been called into question (Hill et al., 2018; Kliewer et al., 2020), prompting us to independently investigate the underlying necessity of ß2-arrestin in mediating ORID. Here, in an experiment where we rigorously control for genetic background, we demonstrate that basal breathing and OIRD are similar in *Arrb2+/+*, *Arrb2*+/-, and *Arrb2*-/- littermates. Furthermore, the *in vitro* preBötC rhythm is similarly silenced by a MOR agonist in all three genotypes. Our data, together with another recent report, does not show a role of *Arrb2* in opioid induced respiratory depression and suggests that MOR biased agonists attenuate OIRD through a different mechanism.

Results

Breathing behaviors and OIRD severity differ between strains of mice (Bubier et al., 2020). Therefore, we sought to compare basal and morphine depressed breathing in mice with the same genetic background. We bred F1 *Arrb2*+/- mice to generate littermates that were wildtype (+/+), heterozygous (+/-), and homozygous (-/-) for germline deletion of *Arrb2* (Figure 3.1A). Breathing was assessed by whole-body plethysmography following intraperitoneal (IP) injection of saline (for control recordings) or after IP morphine (20mg/kg) one day later (Figure 3.1B). This same breathing protocol was conducted in air with 21% O_2 and 0% CO_2 (hereby referred as normoxic) and air with 21% O_2 and 5% CO_2 (hereby referred as hypercapnic). The hypercapnic state

minimizes potential confounding fluctuations in breathing rate and depth seen in normoxic conditions. We used our previously described analytical pipeline (Bachmutsky et al., 2020) to assay the two key parameters that define OIRD, slow and shallow breathing. Slow breathing is measured as the instantaneous frequency of each breath and shallow breathing is defined by the peak inspiratory flow since it strongly correlates with the volume of air inspired (PIF, Figure 3.1C) (Bachmutsky et al., 2020).

In the normoxic condition, the morphology of single breaths, respiratory rate, and peak inspiratory airflow after IP saline appeared similar in *Abbr2*+/+ and -/- mice (Figure 3.2A-B, Table 3.1 contains mean ± SEM and 95% CI). As expected for OIRD, IP morphine decreased the frequency and PIF, but the breathing characteristics remained indistinguishable in *Abbr2*+/+ versus -/- mice (Figure 3.2A-B, Table 3.1). Consistently, histograms of the instantaneous frequency and PIF for each breath after IP morphine showed overlapping distributions from *Arrb2*+/+ (combined from n=5 mice), +/- (n=6), and -/- (n=7) animals (Figure 3.2C, E). We quantified OIRD as the ratio of the average instantaneous frequency or PIF after IP morphine normalized to IP saline. As expected from the raw data, OIRD was similar among the genotypes (rate decreased 60% and PIF by 40%, Figure 3.2D, F, Table 3.2 contains 95% CI for each mean and the comparisons). In fact, there was a small attenuation of respiratory rate depression in *Arrb2*+/+ compared to *Arrb2-/-* and +/- mice, inconsistent with the hypothesis that *Arrb2* mutation attenuates OIRD. These data lead us to conclude that OIRD in normoxic conditions is not diminished in *Arrb2*-/- mice.

These same breathing assays and analysis were also performed in a hypercapnic state. Hypercapnia eliminates any changes in breathing rate and depth that are simply due to variation in behavioral state, like sniffing versus calm sitting. Thus, although breathing when hypercapnic is faster and deeper (like in Figure 3.3A, Table 3.3), the reduced variability minimizes any chance that the conclusions in the normoxic condition are due to additional effects of opioids on behaviors such as sedation and locomotion, or non-opioid-related differences in arousal. Importantly, OIRD

is still robustly observed in the hypercapnic state (Figure 3.3A, Table 3.4). As anticipated, the opioid depression of instantaneous frequency (by ~30%) and PIF (by ~30%) were the same among all three genotypes (Figure 3.3C-F, Table 3.4). Therefore, OIRD is not diminished in *Arrb2*-deficient mice in two independent breathing assays.

To understand the confidence of these results, we determined the extent that *Arrb2*+/+ breathing parameters must be depressed (compared to *Arrb2*-/-) in order to produce a significant test statistic more than 80% of the time, i.e., power analysis. Given our cohort sizes and the observed variation in breathing parameters from *Arrb2*+/+ and -/- littermates, we plotted the relationship between power (0-1) and percent difference between the *Arrb2-/-* and hypothetical *Arrb2*+/+ means (see methods). When comparing the *Arrb2-/-* measured and *Arrb2+/+* hypothetical means, we could confidently distinguish these mean breathing frequencies so long as they differed by at least ~12-20%, and mean PIFs by more than ~10-22% (Figure 3.5). Thus, our experimental approach enabled us to only detect mild to large differences in OIRD between *Arrb2*+/+ and -/- littermates, if they had occurred. It remains possible that a small effect, much smaller than previously reported, was not identified in our study.

The most important site for OIRD is the preBötC (Bachmutsky et al., 2020). So, we directly measured the effects of the opioid peptide [D-Ala, *N*-MePhe, Gly-ol]-enkephalin (DAMGO) on the preBötC rhythm in all three *Arrb2* genotypes. Importantly, DAMGO robustly stimulates both MOR signaling pathways, G-protein and ß2-arrestin dependent signaling. The preBötC slice was prepared from *Arrb2* littermates and the genotype (+/+, +/-, -/-) was determined post hoc. The rhythm was monitored by measuring electrical activity in the hypoglossal nerve rootlet (Smith et al., 1991) for 20 minutes at baseline, and then with 20nM then 50nM DAMGO (Figure 4A-B). The preBötC rhythms of *Arrb2*+/+, +/-, and -/- littermates (n = 5, 20, 6) similarly slowed by ~70-80% at 20nM DAMGO and nearly all were silenced at 50nM (Figure 3.4C-D). If anything, it appears the *Arrb2*-/- slices showed a statistically significant increase in DAMGO sensitivity when compared to *Arrb2*+/- littermates (Figure 3.4C-D), although this likely stems from the differences in cohort sizes

(6 vs. 20). In conclusion, a MOR agonist that substantially activates ß2-arrestin signaling similarly slows the preBötC rhythm in mice lacking the *Arrb2* gene and the littermate controls.

Discussion

The proposed unique importance of MOR-dependent ß2-arrestin signaling in OIRD has motivated the development of biased agonists for analgesia. However, the recent failure to reproduce this result has called model into question (Kliewer et al., 2020). Therefore, the goal of our studies was to test the null hypothesis that germline deletion of *Arrb2* does not attenuate OIRD. The results from our *in vivo* studies under normoxic and hypercapnic conditions, as well as our *in vitro* studies, failed to reject this null hypothesis. In order to directly compare to previous results, we sufficiently powered our cohort size to identify effect sizes reported in Raehal et al., 2005 (~50% less OIRD), and the statistical tests were performed conservatively by not correcting for multiple comparisons. Combined, these three independent assays demonstrate that the germline knockout of *Arrb2* does not attenuate OIRD.

Unlike other studies, we designed ours with five important features to ensure a robust conclusion. First, the OIRD comparisons were made between littermates in an effort to control for any strain specific effects on breathing and opioid sensitivity (Bubier et al., 2020). Second, OIRD was defined as the comparison of breathing after IP injection of saline and morphine in the same animal to control for any within-animal specific breathing variation. Third, we analyzed the multiple breathing parameters with and without averaging across long stretches of breathing. Four, OIRD was measured under a hypercapnic state for a more precise quantification. And fifth, we validated our *in vivo* studies by directly measuring the impact of a MOR ligand on the preBötC rhythm, the key site for OIRD. Future studies should also confirm an unchanged sensitivity to opioids in other brain or peripheral sites that contribute to OIRD.

One difference between our study and the original *Arrb2* study by Raehal et al. was our method of morphine delivery. Raehal et al. reported that at the maximal concentration of morphine

delivered (150mg/kg subcutaneous), the respiratory rate in *Arrb2* knockouts was depressed to half that of wildtype controls (~20% versus 40% depression of breathing rate). In our study, although we delivered 20mg/kg morphine by IP injection, we observed an even larger depression of breathing in all three *Arrb2* genotypes (60% in normoxic and 30% in hypercapnic conditions), indicating our assay was sufficient to observe the reported attenuated OIRD response in *Arrb2*-/- mice. Beyond this, several important future studies to exhaust other methodological limitations include the measurement of respiratory depression in *Arrb2*-/- and littermates with other abused opioids like oxycodone and heroin, to temporally or spatially delete *Arrb2* using *Arrb2*$^{flox/flox}$ alleles to overcome possible compensatory mechanisms, and the study of biased agonists in models where potent opioids like fentanyl are lethal. Additional or other mechanisms may underlie the fatal apnea that was not studied here.

The core premise for the development of MOR biased agonists is that *Arrb2*-dependent signaling provides a molecular mechanism to dissociate analgesia from respiratory depression. Our findings do not support this claim. Consistently, a recent study demonstrated that an opioid receptor ligand that does not induce MOR ß2-arrestin dependent signaling still temporarily induces OIRD (Uprety et al., 2021). Given all of this, how then do some biased agonists show analgesia while minimizing respiratory depression? Perhaps biased agonists are just partial MOR agonists for activation of G-protein signaling. In this case, we imagine analgesia is more sensitive than respiratory depression, and therefore certain concentrations of MOR ligand enable these two effects to be separated. This would be akin to providing a lower dose of standard opioid-like drugs. Regardless, our results, along with similar data from another recent study (Kliewer et al., 2020), refute the foundational model that *Arrb2* selectively mediates OIRD and suggest that now we must reconsider and in the future reinvestigate the mechanism of biased agonism *in vivo.*

Methods

Animals

Arrb2 -/- mice were bred to C57BL/6 to generate heterozygous F1. The F1 littermates were then crossed to make *Arrb2*-/-, *Arrb2*-/+, and *Arrb2*+/+ (F2). Mice were housed in a 12-hour light/dark cycle with unrestricted food and water. Mice were given anonymized identities for experimentation and data collection. All animal experiments were performed in accordance with national and institutional guidelines with standard precautions to minimize animal stress and the number of animals used in each experiment. Institutional Animal Care and Use Committee approval number AN181239.

Plethysmography and respiratory analysis

Plethysmography and respiratory analysis were performed as in (Bachmutsky et al., 2020). Briefly, on the first recording day, adult (6-12 weeks) *Arrb2*-/-, *Arrb2*-/+, and *Arrb2*+/+ mice were administered IP 100μL of saline and placed in an isolated recovery cage for 15 minutes. After, individual mice were then monitored in a 450 mL whole animal plethysmography chamber at room temperature (22°C) in 21% O_2 balanced with N_2 (normoxic condition) or 21% O_2, 5% CO_2 balanced with N_2 (hypercapnic condition). After 1 day, the same protocol was used to monitor breathing after IP injection of morphine (20mg/kg, Henry Schein 057202). The morphine recordings under normoxic and hypercapnic conditions were separated from saline recordings by at least 3 days. Each breath was automatically segmented based on airflow crossing zero as well as quality control metrics. Respiratory parameters (e.g. peak inspiratory flow, instantaneous frequency) for each breath, as well as averages, were then calculated. Reported airflow in mL/sec. is an approximate of true volumes. The analysis was performed with custom Matlab code available on Github with a sample dataset (https://github.com/YackleLab/Opioids-depress-breathing-through-two-small-brainstem-sites). All animals in the study were included in the analysis and cohorts including all these genotypes were run together.

Statistics

A power analysis was performed using the reported effect size from Raehal et al. In this case, 1-4 mice were necessary to observe a statistically significant result. Each cohort (*Arrb2*+/+, +/-, -/-) exceeded 4. Statistical tests were performed on the ratio of IP morphine to IP saline for instantaneous respiratory frequency and peak inspiratory flow separately for normoxic and hypercapnic conditions. A Shapiro Wilks test was first done to determine if the data was normally distributed (Table 3.3 and 3.4). If normal, a single factor ANOVA was performed to determine any differences among the three genotypes (alpha <0.05). In the instance the P-value was <0.05, the Tukey HSD post-hoc test was done to determine which of the pairwise comparisons were statistically different (alpha<0.05). Additionally, one-way unpaired parametric T-tests were used to compare *Arrb2* +/+ and -/- genotypes (alpha<0.05). If the data failed to pass the Shapiro Wilks test, then the non-parametric Kruskal-Wallis test was used to determine if any differences (alpha<0.05). And the Mann-Whitney U test was used to compare *Arrb2*+/+ and -/- genotypes (alpha<0.05). A two-way ANOVA with regression was used to determine interactions between each of the genotypes IP saline and IP morphine values. To determine the power of our data, we compared hypothetical *Arrb2*+/+ and measured *Arrb2*-/- means. The power calculation included our cohort size and the measured standard deviation of the two genotypes. All the above statistics were performed using the publicly available Excel package “Real Statistics Functions” SPSS and Matlab.

Slice electrophysiology

Rhythmic 550 to 650μm-thick transverse medullary slices which contain the preBötC and cranial nerve XII (XIIn) from neonatal *Arrb2* -/-, +/-, +/+ mice (P0-5) were prepared as described (Bachmutsky et al., 2020). Slices were cut in ACSF containing (in mM): 124 NaCl, 3 KCl, 1.5 $CaCl_2$, 1 $MgSO_4$, 25 $NaHCO_3$, 0.5 NaH_2PO_4, and 30 D-glucose, equilibrated with 95% O_2 and 5% CO_2 (4°C, pH=7.4). Recordings were performed in 9 mM at a temperature of 27°C. Slices

equilibrated for 20 min before experiments were started. The preBötC neural activity was recorded from CNXII rootlet. Activity was recorded with a MultiClamp700A or B using pClamp9 at 10000 Hz and low/high pass filtered at 3/400Hz. After equilibration, baseline activity and then increasing concentrations of DAMGO (ab120674) were bath applied (20nM, 50nM). After the rhythm was eliminated, 100nM Naloxone (Sigma Aldrich N7758) was bath applied to demonstrate slice viability. The rate was determined from the last 5 minutes of each 20 minute recording and rhythmic activity was normalized to the first control recording for dose response curves.

Figures

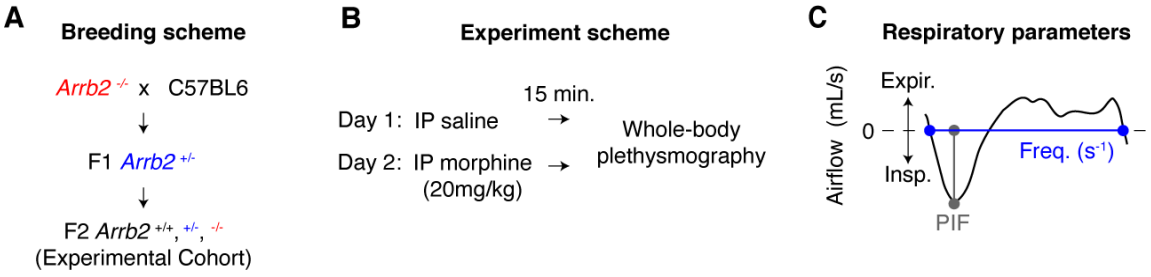

Fig. 3.1. Experimental approach to measure OIRD in each *Arrb2* genotype. **A**, Breeding scheme to generate F2 *Arrb2*+/+, +/-, and -/- littermates. **B**, Whole body plethysmography experimental scheme. On Day 1, recordings were performed 15 minutes after IP saline injection. Day 2, recordings 15 minutes after IP morphine (20mg/kg). Recordings were first conducted under normoxic conditions (21% O_2, 0% CO_2) and then at least one week later under hypercapnic conditions (21% O_2, 5% CO_2). **C**, Example analysis of a single breath. The approximated airflow (mL/s) was used to identify inspiration (insp. <0 mL/s) and expiration (expir. > 0mL/s). Instantaneous frequency (Hz, s^{-1}) defined as the interval between inspiration onset and expiration offset. PIF, peak inspiratory airflow. These two parameters were used to define OIRD.

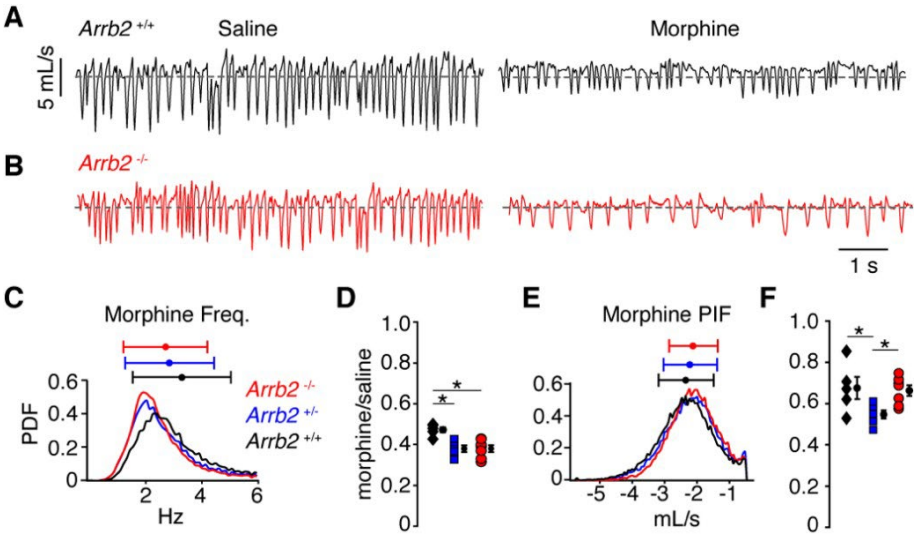

Fig. 3.2. Basal respiration and OIRD in *Arrb2* littermates in normoxic conditions. A, Example breathing trace in normoxic conditions (21% O_2, 0% CO_2) following IP saline (left) and morphine (right) for *Arrb2*+/+. **B**, Example breathing traces from *Arrb2*-/-. **C**, Histogram of instantaneous respiratory frequency (Hz) for all breaths in morphine from *Arrb2*-/- (red, combined from n=7 animals), *Arrb2*+/- (blue, n=6), and *Arrb2*+/+ (black, n=5). PDF, probability density function. Top, mean (circle) ± standard deviation (bars). Values of respiratory measurements are reported in Table 3.1. **D**, OIRD defined as the ratio of average respiratory frequency in morphine to saline for *Arrb2*-/-, *Arrb2*+/-, and *Arrb2*+/+. Mean (circle) ± standard deviation (bars). Data values included in Table 3.2. Note, *Arrb2*+/+ mice have less OIRD when compared to *Arrb2*+/- and -/-. **E-F**, Analysis of peak inspiratory airflow (PIF) displayed as in **C**-**D**. Note, PIF in *Arrb2*+/- mice shows more OIRD when compared to *Arrb2*+/+ and -/-. There is no statistically significant difference between *Arrb2*+/+ and -/-. Single and Two Factor ANOVA and unpaired t-test statistics reported in Table 3.2. *, indicates the post-hoc single factor ANOVA comparisons with P-value <0.05. Statistics were not corrected for multiple comparisons to maximize the possibility of identifying differences between *Arrb2* genotypes.

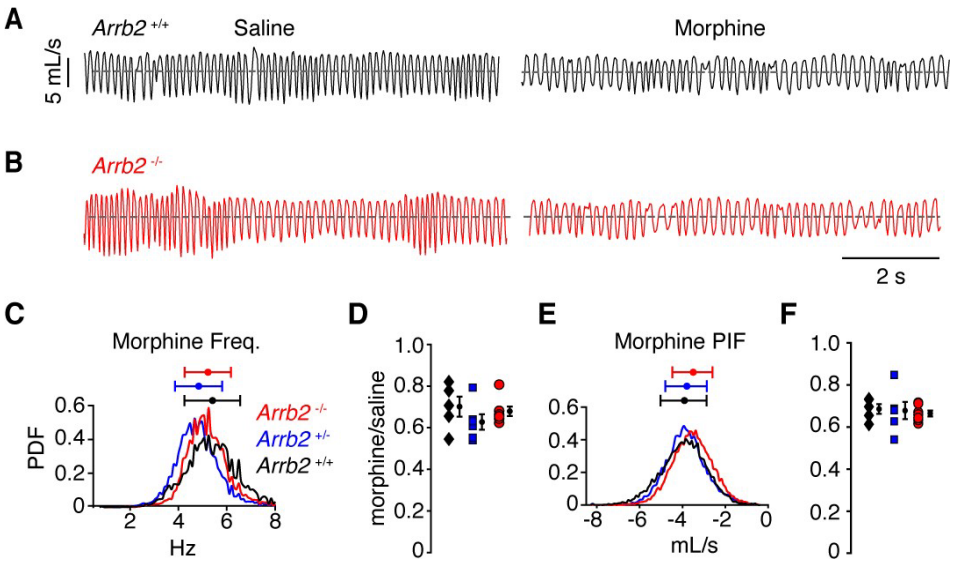

Fig. 3.3. Basal respiration and OIRD in *Arrb2* littermates in hypercapnic conditions. A, Example breathing trace in hypercapnic conditions (21% O_2, 5% CO_2) following IP saline (left) and morphine (right) for *Arrb2*+/+. **B**, Example breathing traces from *Arrb2*-/-. **C**, Histogram of instantaneous respiratory frequency (Hz) for all breaths in morphine from *Arrb2*-/- (red, combined from n=7 animals), *Arrb2*+/- (blue, n=6), and *Arrb2*+/+ (black, n=5). PDF, probability density function. Top, mean (circle) ± standard deviation (bars). Respiratory measurements for saline and morphine are reported in Table 3.3. **D**, OIRD defined as the ratio of average respiratory frequency in morphine to saline for *Arrb2*-/-, *Arrb2*+/-, and *Arrb2*+/+. Mean (circle) ± standard deviation (bars). Data included in Table 3.4. **E-F**, Analysis of peak inspiratory airflow (PIF) as in **C**-**D**. but for peak inspiratory airflow. Single and Two Factor ANOVA and unpaired t-test statistics reported in Table 3.4. Statistics were not corrected for multiple comparisons to maximize the possibility of identifying differences between *Arrb2* genotypes.

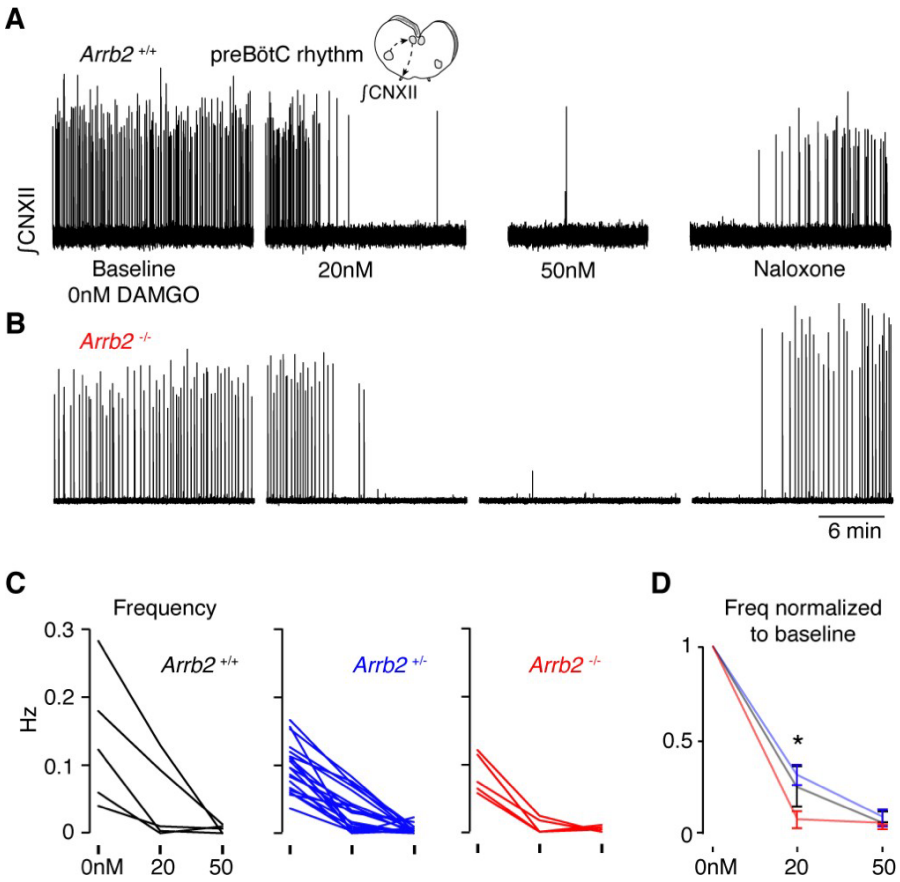

Fig. 3.4. Slowing of preBötC rhythmicity with a MOR agonist from *Arrb2* littermates. A, Neonatal medullary preBötC slice preparation. PreBötC inspiratory activity is measured via the hypoglossal nerve rootlet (∫CNXII, arbitrary units). Example twenty minute recordings from an *Arrb2*+/+ slice where the rhythm is recorded at baseline (0nM DAMGO), then 20nM and 50nM DAMGO, and then with the addition of 100nM Naloxone. **B**, As in **A**, but example recording from an *Arrb2*-/- littermate. **C**, The preBötC frequency (Hz) for each slice from *Arrb2*+/+ (black, n=5), +/- (blue, n=20), and -/- (red, n=6) littermates at each DAMGO dose. Average frequency (bursts per second) is measured during the last five minutes of each recording. **D**, Mean ± SEM for normalized frequency for each genotype at each DAMGO dose. *, p-value <0.05 for Kruskal-Wallis test. P-values for pairwise Mann-Whitney: 0.10 for +/+ vs -/-, 0.45 for +/+ vs +/-, 0.02 for +/- vs -/-.

Tables

Table 3.1. Mean and confidence interval for normoxic condition raw respiratory frequency and peak inspiratory airflow after saline and morphine intraperitoneal injection.

	Arrb2 -/- mean ± SEM	*Arrb2 -/-* 95% CI	*Arrb2 +/-* mean ± SEM	*Arrb2 +/-* 95% CI	*Arrb2 +/+* mean ± SEM	*Arrb2 +/+* 95% CI
Freq. saline (Hz)	7.05 ± 0.34	6.38 → 7.72	7.51 ± 0.41	6.71 → 8.31	6.93 ± 0.32	6.30 → 7.56
Freq. morphine	2.67 ± 0.16	2.36 → 2.98	2.83 ± 0.14	2.56 → 3.10	3.27 ± 0.16	2.96 → 3.58
PIF saline (mL/s)	-3.17 ± 0.15	-2.88 → -3.46	-4.03 ± 0.25	-3.54 → -4.52	-3.5 ± 0.23	-3.04 → -3.95
PIF morphine	-2.09 ± 0.09	-1.91 → -2.23	-2.19 ± 0.10	-1.99 → -2.39	-2.33 ± 0.10	-2.13 → -2.53

Table 3.2. OIRD values of respiratory frequency and peak inspiratory airflow in normoxic conditions and the several types of statistical tests. The respiratory frequency OIRD in *Arrb2*+/+ is larger than *Arrb2*+/- and -/-. The PIF OIRD for *Arrb2*+/- is smaller than *Arrb2*+/+ and -/-.

	Arrb2 -/- OIRD mean (95% CI)	*Arrb2 +/-* mean (95% CI)	*Arrb2 +/+* mean (95% CI)	*Arrb 2 -/-* vs. *Arrb 2 +/+* (t-test)	*Arrb2 -/-* vs. *Arrb2 +/+* (t-test 95% CI)	One-way anov a	Tukey HSD/Kram er *Arrb2 -/-* vs. +/+	Two-way anova regression (interactio n)
Freq .	0.38 (0.35→0.4 1)	0.38 (0.35→0.4 1)	0.47 (0.44→0.5 0)	p = 0.00 1	0.05→0.1 4	0.002	0.003	0.22
PIF	0.66 (0.61→0.7 1)	0.55 (0.48→0.5 6)	0.68 (0.63→0.7 1)	p = 0.83	- 0.13→0.1 6	0.03	0.96	0.05

Table 3.3. Mean and confidence interval for hypercapnic condition raw respiratory frequency and peak inspiratory airflow after saline and morphine intraperitoneal injection.

	Arrb2 -/- mean ± SEM	*Arrb2 -/-* 95% CI	*Arrb2 +/-* mean ± SEM	*Arrb2 +/-* 95% CI	*Arrb2 +/+* mean ± SEM	*Arrb2 +/+* 95% CI
Freq. saline (Hz)	7.68 ± 0.19	7.31 → 8.05	7.69 ± 0.16	7.38 → 8.00	7.77 ± 0.39	7.01 → 8.53
Freq. morphine	5.20 ± 0.10	5.00 → 5.40	4.79 ± 0.19	4.42 → 5.16	5.38 ± 0.18	5.02 → 5.73
PIF saline (mL/s)	-5.34 ± 0.27	-4.81 → -5.87	-5.75 ± 0.25	-5.26 → -6.24	-5.71 ± 0.20	-5.32 → -6.10
PIF morphine	-3.54 ± 0.16	-3.22 → -3.85	-3.86 ± 0.15	-3.57 → -4.15	-3.93 ± 0.24	-3.46 → -4.40

Table 3.4. OIRD values of respiratory frequency and peak inspiratory airflow in hypercapnic conditions and the several types of statistical tests.

	Arrb2 -/- OIRD median or mean (95% CI)	*Arrb2 +/-* mean (95% CI)	*Arrb2 +/+* mean (95% CI)	*Arrb2 -/-* vs. *Arrb2 +/+* (Mann-Whitney or unpaired t-test, two tail)	*Arrb2 -/-* vs. *Arrb2 +/+* (95% CI)	Kruskal-Wallis or One-way anova	Two-way anova - regression (interaction)
Freq.	0.66	0.63 (0.55→0.71)	0.70 (0.60→0.80)	p = 0.52 (MW)	- 0.11→0.15	0.16 (KW)	0.45
PIF	0.66 (0.64→0.68)	0.68 (0.61→0.77)	0.69 (0.64→0.72)	p = 0.46 (t)	- 0.04→0.08	0.86 (anova)	0.96

Table 3.5. Key Resources Table

Key Resources Table				
Reagent type (species) or resource	**Designation**	**Source or reference**	**Identifiers**	**Additional information**
strain, strain background (*Mus musculus*, male and female)	*Arrb2-/-*	The Jackson Laboratory	011130	
strain, strain background (*Mus musculus*, male and female)	C57Bl/6J	The Jackson Laboratory	000664	
peptide, recombinant protein	DAMGO	Abcam	Ab12067	
chemical compound, drug	Morphine sulfate	Henry Schein	057202	
chemical compound, drug	Naloxone	Sigma Aldrich	N7758	
software, algorithm	Matlab	Mathworks		https://github.com/YackleLab/Opioids-depress-breathing-through-two-small-brainstem-sites

Supplemental Figures

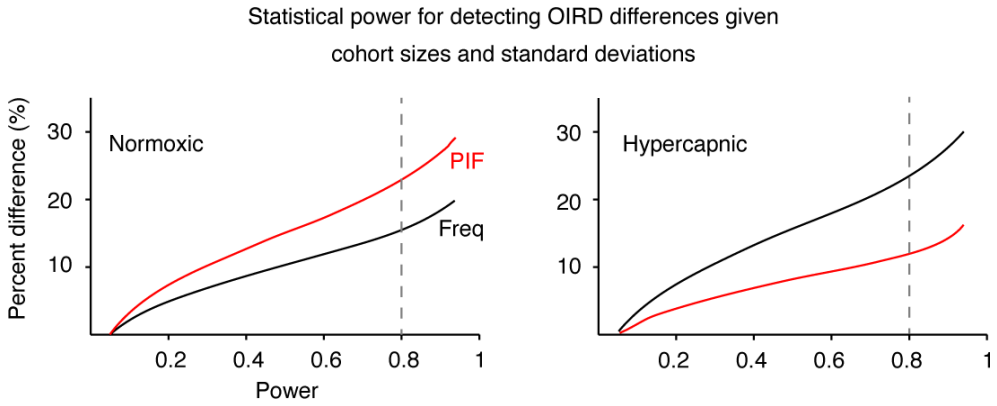

Fig. 3.5 (Figure 3 – Supplement 1). Power analysis to determine the OIRD effect size given the cohort sizes and data in normoxic and hypercapnic experimental conditions. A power analysis was conducted with the hypothetical mean frequency and peak inspiratory airflow (PIF) of *Arrb2*+/+ compared to the measured mean from *Arrb2*-/-. The power analysis used the cohort size and measured standard deviation of *Arrb2*+/+ and -/-. Displayed is the percent difference in OIRD between *Arrb2*-/- and +/+ (y-axis) at each power (x-axis). Respiratory frequency (Freq, black). Peak inspiratory airflow (PIF, red). Right, Normoxic condition. Left, Hypercapnic condition. Gray dashed line, power of 0.8.

References

1. Al-Hasani R, Bruchas MR. 2011. Molecular mechanisms of opioid receptor-dependent signaling and behavior. *Anesthesiology* **115**:1363–1381. doi:10.1097/aln.0b013e318238bba6.
2. Bachmutsky I, Wei XP, Kish E, Yackle K. 2020. Opioids depress breathing through two small brainstem sites. *eLife* **9**. doi:10.7554/elife.52694.
3. Bohn LM, Lefkowitz RJ, Gainetdinov RR, Peppel K, Caron MG, Lin F-T. 1999. Enhanced Morphine Analgesia in Mice Lacking Beta-Arrestin 2. *Science* **286**:2495–2498. doi:10.1126/science.286.5449.2495.
4. Bubier JA, He H, Philip VM, Roy T, Hernandez CM, Donohue KD, O'Hara BF, Chesler EJ. 2020. Genetic Variation Regulates Opioid-Induced Respiratory Depression in Mice. *Sci Rep.* **10**:14970. doi:10.1038/s41598-020-71804-2.
5. Calebiro D, Nikolaev VO, Persani L, Lohse MJ. 2010. Signaling by internalized G-protein-coupled receptors. *Trends Pharmacol Sci* **31**:221–228. doi:10.1016/j.tips.2010.02.002.
6. Dahan A, Sarton E, Teppema L, Olievier C, Nieuwenhuijs D, Matthes HW, Kieffer BL. 2001. Anesthetic potency and influence of morphine and sevoflurane on respiration in mu-opioid receptor knockout mice. *Anesthesiology* **94**:824–832. doi:10.1097/00000542-200105000-00021.
7. Hill R, Disney A, Conibear A, Sutcliffe K, Dewey W, Husbands S, Bailey C, Kelly E, Henderson G. 2018. The novel μ-opioid receptor agonist PZM21 depresses respiration and induces tolerance to antinociception. *British journal of pharmacology* **175**:2653–2661. doi:10.1111/bph.14224.
8. Kliewer A, Gillis A, Hill R, Schmiedel F, Bailey C, Kelly E, Henderson G, Christie MJ, Schulz S. 2020. Morphine-induced respiratory depression is independent of β-arrestin2 signaling. *Brit J Pharmacol* **177**:2923–2931. doi:10.1111/bph.15004.

9. Luttrell LM, Lefkowitz RJ. 2002. The role of beta-arrestins in the termination and transduction of G-protein-coupled receptor signals. *Journal of cell science* **115**:455–465.
10. Manglik A, Lin H, Aryal DK, McCorvy JD, Dengler D, Corder G, Levit A, Kling RC, Bernat V, Hübner H, Huang X-P, Sassano MF, Giguère PM, Löber S, Duan D, Scherrer G, Kobilka BK, Gmeiner P, Roth BL, Shoichet BK. 2016. Structure-based discovery of opioid analgesics with reduced side effects. *Nature* **537**:185–190. doi:10.1038/nature19112.
11. Montandon G, Ren J, Victoria NC, Liu H, Wickman K, Greer JJ, Horner RL. 2016. G-protein-gated Inwardly Rectifying Potassium Channels Modulate Respiratory Depression by Opioids. *Anesthesiology* **124**:641–650. doi:10.1097/aln.0000000000000984.
12. Pattinson KTS. 2008. Opioids and the control of respiration. *British Journal of Anaesthesia* **100**:747–758. doi:10.1093/bja/aen094.
13. Raehal KM, Walker JKL, Bohn LM. 2005. Morphine Side Effects in β-Arrestin 2 Knockout Mice. *J Pharmacol Exp Ther* **314**:1195–1201. doi:10.1124/jpet.105.087254.
14. Schmid CL, Kennedy NM, Ross NC, Lovell KM, Yue Z, Morgenweck J, Cameron MD, Bannister TD, Bohn LM. 2017. Bias Factor and Therapeutic Window Correlate to Predict Safer Opioid Analgesics. *Cell* **171**:1165-1175.e13. doi:10.1016/j.cell.2017.10.035.
15. Scholl L, Seth P, Kariisa M, Wilson N, Baldwin G. 2018. Drug and Opioid-Involved Overdose Deaths - United States, 2013-2017. *MMWR Morbidity and mortality weekly report* **67**:1419–1427. doi:10.15585/mmwr.mm675152e1.
16. Smith JC, Ellenberger HH, Ballanyi K, Richter DW, Feldman JL. 1991. Pre-Bötzinger complex: a brainstem region that may generate respiratory rhythm in mammals. **254**:726–729. doi:10.1126/science.1683005.
17. Turnaturi R, Chiechio S, Salerno L, Rescifina A, Pittalà V, Cantarella G, Tomarchio E, Parenti C, Pasquinucci L. 2019. Progress in the development of more effective and safer analgesics for pain management. *Eur J Med Chem* **183**:111701. doi:10.1016/j.ejmech.2019.111701.

18. Uprety R, Che T, Zaidi S, Grinnell S, Varga B, et al. 2021. Controlling opioid receptor functional selectivity by targeting distinct subpockets of the orthosteric site. *Elife* 10:e56519. doi: 10.7554/eLife.56519.
19. Varga AG, Reid BT, Kieffer BL, Levitt ES. 2019. Differential impact of two critical respiratory centers in opioid-induced respiratory depression in awake mice. *The Journal of physiology* JP278612-37. doi:10.1113/jp278612.
20. Wei AD, Ramirez J-M. 2019. Presynaptic Mechanisms and KCNQ Potassium Channels Modulate Opioid Depression of Respiratory Drive. *Frontiers in physiology* **10**:1407. doi:10.3389/fphys.2019.01407.
21. Zurawski Z, Yim YY, Alford S, Hamm HE. 2019. The expanding roles and mechanisms of G protein-mediated presynaptic inhibition. *Journal of Biological Chemistry* **294**:1661–1670. doi:10.1074/jbc.tm118.004163.

Chapter 4:

Conclusions

This work has defined the brain areas, cell-types, and molecular mechanisms mediating opioid-induced respiratory depression, in the hopes that this understanding will fuel the development of novel therapeutics that prevent overdose.

Opioids depress breathing through two small brainstem sites

By rigorously quantifying opioid depressed breathing before and after local knockout of the opioid receptor, I show that two small brainstem sites mediate lethal overdose: the preBötzinger Complex (preBötC) and the Parabrachial Nucleus. I find that the critical site is the breathing pacemaker, the preBötC, and used genetic tools and *in vitro* electrophysiology to reveal that just 70–140 neurons in this region (just 5% of all neurons) are responsible for its sensitivity to opioids.

Future work will dissect the role of these 140 neurons in awake animals and determine whether these neurons play a critical role in breathing rhythmogenesis.

ß-arrestin 2 germline knockout does not attenuate opioid respiratory depression

The novel development of ‘biased agonist’ opioid drugs promised to dissociate negative lethal effects of opioids, due to depression of breathing, from their positive analgesic effects. This bold idea was founded on a claim that opioid induced slow breathing was mediated by the downstream ß-arrestin 2 signaling pathway. By re-examining this claim in ß-arrestin 2 deficient mice I found no connection between the ß-arrestin 2 signaling pathway and opioid respiratory depression. This suggests any therapeutic benefit of ‘biased agonists’ must work through a yet to be identified mechanism.

Various groups are currently investigating whether ß-arrestin 2 signaling is critical in the development of tolerance to opioid drugs, and some claim that these ‘biased agonist’ drugs may still have some future as therapeutics by preventing tolerance. This is still up for debate.

Regardless, the future of this strategy to directly prevent overdose is bleak and this work suggests that we must pursue new strategies in the development of safer opioid drugs.

Another interesting observation is that while opioids are highly potent drugs, people who take antagonists that target these same receptors report no noticeable changes. This suggests that the endogenous opioid peptides these drugs mimic are likely released only in selective contexts that have yet to be discovered. Because breathing provides a highly quantifiable, opioid-sensitive readout it can be used to screen potential behavioral contexts.

In general, the breathing pacemaker expresses a wide variety of endogenous neuropeptide receptors and I believe future work could use this platform to discover basic principles underpinning the dynamics of neuropeptide modulation.

Publishing Agreement

It is the policy of the University to encourage open access and broad distribution of all theses, dissertations, and manuscripts. The Graduate Division will facilitate the distribution of UCSF theses, dissertations, and manuscripts to the UCSF Library for open access and distribution. UCSF will make such theses, dissertations, and manuscripts accessible to the public and will take reasonable steps to preserve these works in perpetuity.

I hereby grant the non-exclusive, perpetual right to The Regents of the University of California to reproduce, publicly display, distribute, preserve, and publish copies of my thesis, dissertation, or manuscript in any form or media, now existing or later derived, including access online for teaching, research, and public service purposes.

DocuSigned by:
Iris Bachmutsky
F01F1511E8AF4C1...
Author Signature

12/12/2022
Date